



Old and New Methods of Glaucoma Diagnosis Using Spectral-Domain Optical Coherence Tomography: Testing Limitations of Older Retinal Nerve Fiber Layer Thickness Measurements and Diagnostic Potential of Newer Retinal Volume Measurements

Citation

Liu, Yingna. 2017. Old and New Methods of Glaucoma Diagnosis Using Spectral-Domain Optical Coherence Tomography: Testing Limitations of Older Retinal Nerve Fiber Layer Thickness Measurements and Diagnostic Potential of Newer Retinal Volume Measurements. Doctoral dissertation, Harvard Medical School.

Permanent link

<http://nrs.harvard.edu/urn-3:HUL.InstRepos:32676131>

Terms of Use

This article was downloaded from Harvard University's DASH repository, and is made available under the terms and conditions applicable to Other Posted Material, as set forth at <http://nrs.harvard.edu/urn-3:HUL.InstRepos:dash.current.terms-of-use#LAA>

Share Your Story

The Harvard community has made this article openly available.
Please share how this access benefits you. [Submit a story](#).

[Accessibility](#)

TABLE OF CONTENTS

Abstract.....	2
Glossary.....	4
1. Introduction.....	5
Part I	
2. Methods.....	11
3. Results.....	14
4. Discussion.....	18
Part II	
5. Methods.....	25
6. Results.....	27
7. Discussion.....	30
8. Future directions.....	35
9. Summary.....	37
References.....	38
Figures and Tables.....	46

ABSTRACT

Purpose:

Optical coherence tomography (OCT) retinal nerve fiber layer (RNFL) thickness measurements are a reproducible and quantitative diagnostic modality widely used for glaucoma evaluations, but a high rate of testing artifacts limits its clinical utility. In Part I of this thesis, we aimed to characterize artifact types and assess artifact rates in two-dimensional (2D) RNFL thickness measurements obtained by the Spectralis OCT machine (Heidelberg Engineering, Heidelberg, Germany), as well as to determine patient factors and eye conditions associated with a higher artifact prevalence. In Part II of this thesis, we aimed to compare a new parameter, peripapillary retinal volume (RV), with the traditional 2D RNFL thickness parameter for diagnostic capability and artifact rates.

Methods:

Part I: The prevalence of 12 artifact types were described in this retrospective, cross-sectional review of 2313 eye scans from 1188 patients who underwent a complete eye examination with Spectralis OCT scanning during the period of September 2009 to July 2013. Generalized estimating equations model was used to analyze associations between increased artifact prevalence and 10 patient characteristics, including age, sex, race, visual acuity, refractive error, astigmatism, cataract status, glaucoma staging, visual field reliability, and glaucoma diagnosis.

Part II: This is a retrospective, cross-sectional review. A total of 180 subjects [113 open angle glaucoma (OAG) and 67 normal participants] had spectral domain optical coherence tomography (OCT) volume scans and RNFL thickness measurements (Spectralis, Heidelberg Engineering, Heidelberg, Germany). Peripapillary RV values were calculated using a custom-designed program with 4 different sized circumpapillary annuli (CA): CA1 had circle diameters of 2.5 and 3.5 mm; CA2, 3 and 4 mm; CA3, 3.5 and 4.5 mm; and CA4, 4 and 5 mm. Area under the receiver operating characteristic (AUROC) curves, sensitivity, and specificity were calculated for global, quadrant, and octant regions for RV (CA1 – CA4) and RNFL thickness. Pair-wise comparisons were conducted between RV and RNFL measurements. Artifacts rates were determined.

Results:

Part I: A total of 1070 or 46.3% of the 2313 2D eye scans had at least one artifact. Decentration error was the most common artifact (27.8%), followed by posterior vitreous detachment artifacts (14.4%). Visual acuity of less than 20/40 ($p < 0.0001$), presence of moderate to severe cataracts ($p < 0.0001$), advanced stage of glaucoma ($p < 0.0001$), and a diagnosis of open angle glaucoma ($p = 0.0003$) were associated with increased prevalence of artifacts.

Part II: Of the 180 study subjects who had 3D eye scans, mean age was 62.6 ± 15.4 years and 41.7% were male. Among RV measurements, best diagnostic performances were for the smallest two annuli for inferior RV (CA1 0.964, CA2 0.955). Of the 4 annuli, the smallest CA1 had the highest diagnostic performance. Of specific regions, the inferior RV quadrant had the highest performance across CA1 to CA4. Peripapillary RV had similar diagnostic capability compared to RNFL thickness ($p > 0.05$). The artifact rate per B-scan for RV was 6.0%, and for 2D RNFL thickness scans was 32.2%.

Conclusions:

Clinicians should first assess scans for artifacts and pay attention to patient characteristics associated with a higher prevalence of artifacts before making therapeutic decisions based on RNFL thickness measurements. Meanwhile, the diagnostic capability of RV could be equal to that of RNFL thickness for diagnosing perimetric OAG, with fewer artifacts. RV may be a useful novel parameter in the evaluation of perimetric glaucoma.

GLOSSARY

2D: Two-dimensional

3D: Three-dimensional

AUROC: Area under the receiver operating characteristic

CA: Circumpapillary annulus

CI: Confidence interval

ETDRS: Early treatment for diabetic retinopathy study

IN: Inferior-nasal

IT: Inferior-temporal

MD: Mean deviation

MDB: Minimum distance band

NPV: Negative predictive value

NLR: Negative likelihood ratio

OAG: Open-angle glaucoma

OCT: Optical coherence tomography

PCIOL: Posterior chamber intraocular lens

PLR: Positive likelihood ratio

PPA: Peripapillary atrophy

PPV: Positive predictive value

PVD: Posterior vitreous detachment

RNFL: Retinal nerve fiber layer

RPE: Retinal pigment epithelium

RV: Retinal volume

SD-OCT: Spectral domain optical coherence tomography

SE: Spherical equivalent

SN: Superior-nasal

ST: Superior-temporal

TD-OCT: Time domain optical coherence tomography

VA: Visual acuity

VF: Visual field

1. INTRODUCTION

1.1. The disease: glaucoma

Glaucoma is the leading cause of irreversible blindness in the world, and among populations of European and African descent, open-angle glaucoma (OAG) is the most common type.^{1,2} OAG affected an estimated 57.5 million people worldwide in 2015, and this number is projected to increase to 65.5 million by 2020.³ In the United States alone, more than 2.8 million people are living with OAG,⁴ and this number will increase to 3.4 million in 2020.⁵ The overall prevalence of OAG is estimated to be 1.86% in men 40 years or older.⁵ This number is an underestimate since half of the individuals with glaucoma, even in developed countries, remain undiagnosed.⁶

Open-angle glaucoma is an optic neuropathy characterized by the death of retinal ganglion cells and the optic nerve or “disc” takes on a hollowed-out appearance.⁷ As a result, glaucoma causes irreversible loss of vision. Therefore, the goal of glaucoma management is to diagnose this disease at an early stage and initiate treatment to stop or slow down further vision loss. However, OAG is challenging to diagnose at an early stage because patients are asymptomatic early on, and even in advanced stages, vision loss may not be noticeable, since loss of vision is gradual and starts from the periphery.

Conventional diagnosis of OAG is defined by the clinical appearance of the optic nerve and an interpretation of peripheral visual field testing. It relies on a combination of fundus examination, visual field testing, and intraocular pressure measurements that altogether provide a clinical diagnosis. However, these tests are limited because 1) they rely on the subjective test response of the patient, such as the visual field test, 2) they rely on the subjective interpretation of the test by the physician, and 3) they do not allow diagnosis of glaucoma before optic disc cupping and/or vision field loss develop. Indeed, it was estimated that the current clinical “gold standards” can diagnose glaucomatous vision loss only after up to 40% of the nerve tissue is lost irreversibly.⁸

Since timely initiation of treatment can be vision saving,⁹ a reliable diagnostic tool for OAG has important public health implications. In particular, driven by the need to diagnose glaucoma not only earlier but also in a more objective manner, imaging techniques such as optical coherence tomography (OCT) has been developed in an attempt to measure objectively and quantitatively changes in both the optic nerve head

(ONH) and the retinal nerve fiber layer (RNFL), both of which undergo structural changes with glaucoma. In the past decade, OCT measurement of RNFL has emerged to the forefront of glaucoma imaging due to its high resolution, the complex 3D data it gathers, and its ability to provide reproducible measurements.

1.2. Optical coherence tomography (OCT) and RNFL measurements

First developed and described in 1991 by Huang et al,¹⁰ optical coherence tomography (OCT) is a noninvasive imaging technique that uses low-coherence interferometry to generate high-resolution cross-sectional images of any optically accessible tissue. OCT imaging has undergone many significant technological advances, and current commercially available spectral domain OCT (SD-OCT) machines, such as the Spectralis OCT (Heidelberg Engineering, Heidelberg, Germany), provide ultra-high speed images, with better resolution and sensitivity compared to older time domain OCT (TD-OCT) devices.¹¹

One of the anatomical hallmarks of glaucoma is thinning of the retinal nerve fiber layer (RNFL), which are the axons of retinal ganglion cells, the death of which lead to vision loss in glaucoma.¹² Automated SD-OCT measurements allow for quantitative and objective assessments of early RNFL thinning, which can be detected before corresponding visual field loss.^{8,13,14} Numerous studies have demonstrated that RNFL thickness parameters by OCT are not only reproducible but also have high diagnostic sensitivity and specificity in discriminating between glaucomatous versus healthy eyes.¹⁵⁻¹⁹ One study found that RNFL thickness measurements using SD-OCT had an area under receiver operating characteristics curve (AUROC) value of approximately 0.9.²⁰

Based on the above clinical data, the use of SD-OCT for glaucoma diagnosis has become a common practice. In fact, RNFL thickness measurement by SD-OCT is the most commonly measured OCT parameter in glaucoma. However, SD-OCT, or any test, is limited by the quality of the test. Errors either in data acquisition or software analysis may result in erroneous RNFL measurements, which may lead to an inaccurate clinical assessment. SD-OCT has been reported to have a decreased incidence of segmentation errors compared to older TD-OCT devices.^{21,22} Han and Jaffe performed a study to characterize the types and frequencies of image artifacts with Cirrus SD-OCT

imaging of the macula for the evaluation of retinal diseases.²³ Several types of artifacts were observed, including inner and outer retina misidentification, degraded scan images, cut edge artifacts, incomplete segmentation errors, and retinal image shifts. As many as 90.9% of scans had at least 1 artifact, and clinically significant artifacts were observed in 8.0% of scans.²³ Asrani et al conducted a retrospective cross-sectional study on 277 consecutive patients with a diagnosis of glaucoma and obtained Spectralis OCT scanning of the RNFL.²⁴ They found that 19.9% of RNFL scans contained artifacts, and the most common cause of artifacts was related to epiretinal membranes. While these previous studies provided invaluable insight to the artifact rates and types in OCT imaging, no prior study has been conducted to specifically investigate patient factors or eye conditions associated with a higher prevalence of artifacts in SD-OCT imaging of the RNFL thickness in glaucoma.

In addition to artifacts, the reliability of RNFL measurements also decreases in glaucoma when RNFL is thinner,^{25(p),26} which is related to the decreased reflectivity of RNFL in glaucoma, making it difficult for segmentation algorithms to differentiate the normally highly reflective RNFL from underlying tissue.²⁷ Furthermore, decreased RNFL thickness is seen in eye pathologies other than glaucoma. For example, high myopia, or longer axial lengths, can be independently associated with thinner RNFL thickness unrelated to glaucoma.²⁸⁻³² Also, peripapillary atrophy (PPA), a common pathology associated with myopia, is associated with the absence of retinal layers,³³ and as a result, decreased diagnostic performance of RNFL thickness for glaucoma.^{34,35} Overall, the rate of false positives when using Spectralis OCT to measure RNFL thickness in glaucoma has been reported to be as much as around 18%.³⁵

1.3. New OCT measurements in glaucoma

Due to the aforementioned limitations of RNFL thickness measurements in glaucoma, such as decreased RNFL reflectivity, and in myopia and PPA, other OCT measurements have been investigated for their diagnostic use and artifact rates.

For example, the minimum distance band (MDB) neuroretinal rim measurement, which is derived from high-density OCT volume scans, has been shown by colleagues in our research group to have equal or superior diagnostic capability compared to 2D RNFL thickness measurements.^{36,37} The MDB is the 3D region delimited by the

shortest distances between the internal limiting membrane (ILM) and the optic disc margin, presumed to be the retinal pigment epithelium (RPE)/Bruch's membrane complex termination.^{38,39} Among a total of 163 patients, only 10 patients had volumes scans that the segmentation program failed to correctly process, which gives an estimated artifact rate of around 6.1%.

Furthermore, our group has explored the diagnostic potential of retinal thickness (RT) measurements from 3D volume scans for glaucoma diagnosis. RT measurements were determined by centering the early treatment for diabetic retinopathy study (ETDRS) circular grid over the optic nerve, and it was shown to have the same or better diagnostic capability compared to peripapillary RNFL thickness but with fewer segmentation errors.⁴⁰

In contrast to peripapillary RT measurements, peripapillary retinal volume (RV) measurements offer three-dimensional information as opposed to two-dimensional data, and therefore, may detect more subtle changes in the anatomy over time. Macular RV has previously been studied in the context of neovascular macular degeneration and retinoschisis.^{41,42} More recently, our group showed that peripapillary RV measurements using ETDRS circular grids also had excellent diagnostic capability and significantly lower artifact rates compared to RNFL thickness.⁴³

1.4. Rationale

Peripapillary 2D RNFL thickness measurements by SD-OCT, while offering objective, quantitative and reproducible data to facilitate clinical assessment of glaucoma, is limited by artifacts, as discussed above.^{23,24} Because it is widely used in the diagnosis and follow-up of glaucoma in current practice, understanding of artifacts in SD-OCT peripapillary RNFL measurements, and in particular, artifact rate, artifact types and the patient population most affected by artifacts are critical in the clinical assessment of this important imaging technique.

Part I of this thesis, therefore, sought to evaluate artifacts in the modality of 2D RNFL measurement by SD-OCT, by 1) characterizing artifact types, 2) assessing artifact rates, 3) evaluating if RNFL artifacts were associated with patient factors or eye conditions in a large patient population of almost 1200 patients. We hypothesized that an increased prevalence of RNFL artifacts in Spectralis OCT imaging is associated with

patient factors such as older age, female gender, worse visual acuity, worsen refractive error and astigmatism, and worse glaucoma severity.

In addition to understanding the limitations of 2D RNFL thickness, we also sought to evaluate new OCT measurements that would not only offer equal or superior diagnostic performance in glaucoma evaluation, but with less limitations, for example, with lower rates of artifacts.

RT and RV measurements from 3D SD-OCT volume scans were previously demonstrated to have excellent diagnostic performance with lower artifact rates.^{40,43} In these two studies, ETDRS circular grid and its set dimensions (diameters of 1, 2, 3 mm; 1, 2.22, 3.45 mm; and 1, 3, 6 mm) were used since it was already built into the Heidelberg system for macular imaging. Because of these promising results, our group developed software to measure peripapillary retinal volume using a new set of circumpapillary annuli, whose inner and outer diameters could be varied to any diameter. We customized annular sizes, different from regions on the EDTRS grid, to specifically capture glaucomatous peripapillary changes.

Therefore, Part II of this thesis sought to compare the diagnostic capability of 3D peripapillary retinal volume measurements from 3D volume scans for open-angle glaucoma versus that of 2D RNFL thickness measurements. We hypothesized that RV measurements from Spectralis OCT scans, using customized annular sizes, have equal or better diagnostic capabilities compared to peripapillary RNFL thickness in OAG patients.

Part I

Evaluation of Artifacts in Spectralis Optical Coherence Tomography Imaging of the Retinal Nerve Fiber Layer in Glaucoma and Patient Characteristics Associated with Artifacts

2. METHODS

2.1. Study population

A retrospective review of patients and their eye scans was conducted with approval from the Massachusetts Eye and Ear Infirmary (MEEI) Institutional Review Board, and the study protocol was in accordance with the Health Insurance Portability and Accountability Act.

Subjects were included in the study if they were seen in the Glaucoma Service at MEEI (by Dr. Teresa Chen) and underwent a complete eye exam with Spectralis OCT scanning during the period of September 2009 to July 2013. A total of 1188 patients met the above criteria and were included in the study. Some patients had multiple scans, but only the most recent SD-OCT Spectralis scans were used for the study. Both eyes were included in the study if a patient had both eyes scanned. Sixty-three patients only had scans from one eye, so only one scan for these patients was included. As a result, a total of 2313 eye scans were reviewed in this study.

2.2. Spectralis OCT imaging of RNFL in 2D eye scans

All patients had peripapillary SD-OCT RNFL thickness measured using a circular scan pattern.^{26,44} The Spectralis OCT is an SD-OCT machine that has a scan speed of 40,000 A-lines per second and an eye tracking system, the TruTrack™ image alignment software, which reduces target motion artifacts and results in more stable captured images. The scan automatically generates a quality score of 0 to 40 decibels (dB). Multiple frames at the same location are obtained and then averaged to reduce speckle noise. The scan circle around the optic nerve is 12 degrees in diameter, and the scan circle diameter in millimeters therefore depends on the axial length. For a typical eye length, the circle would be approximately 3.5 to 3.6 mm in diameter. Scans were acquired in High Speed mode.

The Spectralis OCT software (version 4.0) allows for automatic segmentation of the anterior and posterior borders of the RNFL to calculate the average RNFL thickness for the overall global (360 degrees), for 4 quadrants (superior [S], inferior [I], nasal [N], and temporal [T]), and for four additional sectors (superior-temporal [ST, 45-90 degrees], superior-nasal [SN, 90-135], inferior-nasal [IN, 225-270 degrees], and inferior-temporal [IT, 270-315]).

2.3. Evaluation of imaging artifacts

In this study, we defined 12 artifact types. A type 1 artifact was defined as algorithm failure or incorrect segmentation of the anterior RNFL (Figure 1, white arrow), and a type 2 artifact occurred when there was posterior RNFL misidentification (Figure 1 and Figure 2, yellow arrows). A type 3 artifact occurred when there was incomplete segmentation (Figure 3), when the algorithm failed to delineate the entire extent of the RNFL, or when the red line on the OCT printout ended before the OCT image ended. Complete absence of segmentation was considered a subtype of artifact type 3.

Spectralis OCT scans were considered de-centered (type 4, Figure 4) when the center of the optic nerve head was more than approximately 10% off the center of the peripapillary circular scan. Spectralis SD-OCT automatically generates a quality score from 0 to 40 dB. Type 5 or poor signal artifact (Figure 5, yellow arrow) was defined as a quality score of less than 15, as indicated in the Spectralis user's manual.⁴⁵ A type 6 artifact (Figure 6, yellow arrow) occurred when part of the scan was missing and when a portion of the RNFL across its entire thickness was completely black or indistinguishable from the background noise. Since glaucoma patients tend to have decreased RNFL thickness, cases where even the slightest signal above background noise was detected were excluded as an artifact. Type 7 cut edge artifacts (Figure 7, yellow arrows) were identified in cases of abrupt lateral edge truncation of the RNFL. Type 8 motion artifacts (Figure 8) were due to patient movement during scanning. If patient movement caused parts of the OCT scan to be completely out of the rectangular display printout, this was counted as a movement artifact. If the OCT scan was characterized by a wavy or undulating appearance of the entire scan image but if the entire retina was still visible in the displayed scan, this was not considered a motion artifact in this paper.

Patient ocular pathology-associated artifacts types 9 to 12 were identified when the RNFL scan circle involved scanning over areas of clinically documented fundus abnormalities. Type 9 posterior vitreous detachment (PVD) associated artifacts (Figure 9, yellow arrow) were identified in scans where a clear PVD was present on the Spectralis OCT printout. Type 10 was a peripapillary atrophy (PPA) associated artifact (Figure 10, yellow arrow). Type 11 was a staphyloma-associated artifact (Figure 11,

yellow arrow). Type 12 was a myelinated nerve fiber layer (MNFL)-associated artifact (Figure 12, yellow arrow).

2.4. Patient factors and eye characteristics

We recorded patient specific factors such as age, sex, race, as well as eye specific factors such as visual acuity (VA), refractive error [with spherical equivalent (SE)], astigmatism (cylindrical refractive errors), cataract status, glaucoma diagnosis, glaucoma staging, and visual field reliability.

Visual acuity was either best corrected visual acuity (cc) or visual acuity without correction (sc) if visual acuity did not improve with correction. Vision was divided into two categories: 1) 20/40 or better, and 2) worse than 20/40.

Refraction, if recorded within 3 months of the OCT scan, was included in this study. If there were multiple refractions, the one closest to the date of the scan was used. Of the 2313 eye scans, 1091 eye scans did not have any documented refraction within the 3 month time period. For the remaining 1222 eye scans, patients were categorized as being either within -6.00 diopters (D) SE to +5.00 D SE, inclusive, or worse than -6.00 D SE or worse than +5.00 D SE. Astigmatism was evaluated, and patients were categorized as either better than or equal to +/-3.00 D of cylinder, or worse than +/- 3.00 D of cylinder.

Cataract status was evaluated on the day of the Spectralis scan and was classified as being: 1) clear, no cataract, 2) trace to 1+ cataract, 3) 2+ cataract or more, or 4) with a posterior or anterior chamber intraocular lens. If a patient had glaucoma, glaucoma staging was evaluated based on the mean deviation (MD) value from Humphrey visual field testing (SITA-standard 24-2 strategy, model HFAII series 750i, Carl Zeiss Meditec Inc., Jena, Germany), and glaucoma stages were classified using a modified Hodapp-Anderson-Parrish system which graded fields as 1) normal ($MD \geq 0$), 2) mild ($-6 \leq MD < 0$), 3) moderate ($-12 \leq MD < -6$), or 4) advanced ($MD < -12$). Visual fields were categorized as reliable, if false positives were $\leq 20\%$, false negatives $\leq 20\%$, and fixation losses $\leq 33\%$. Patients were also categorized according to their glaucoma diagnosis. The four most common glaucoma diagnoses each were categorized into their own individual groups; pediatric glaucoma was categorized as a separate group, and the rest of the diagnoses were included in the category of "other."

2.5. Statistical analysis

All statistical analysis was performed using SAS version 9.3 (Cary, NC). To quantify the frequency of artifacts among all scans analyzed, the number of scans with at least one artifact was divided by the total number of scans. Scans that had multiple artifacts were only counted once. Analyses were then performed for each artifact type. The frequencies of scans with 1, 2, and 3 or more types of different artifacts were also quantified by dividing the number of corresponding scans by the total number of scans analyzed.

Statistical analyses were performed on a per-eye basis to assess the effects of patient-specific and eye-specific factors on the prevalence and frequency of artifacts in SD-OCT imaging. Generalized estimating equation models were used to account for correlations of the paired eyes of the same subjects. Bivariate analyses were first conducted to determine the existence of association between each of the patient and eye specific factors (age, sex, race, visual acuity, refractive error, astigmatism, cataract status, glaucoma staging, visual field reliability, glaucoma diagnosis) and the frequency of eye scans with at least one artifact. Variables with a bivariate significance of $p < 0.10$ were selected for the multivariate model building. Glaucoma diagnosis and glaucoma staging were highly correlated and therefore they were not entered in a model simultaneously.

A manual selection method was utilized, and those maintaining a $p < 0.05$ were kept. The bivariate predictors not included in the model were manually re-entered for an assessment of confounding effects. Interaction effects with the significant variables were also assessed. All missing data was excluded from analysis. Of note, 1091 eye scans did not have a recorded refraction, so bivariate analyses were carried out with the remaining 1222 eye scans as a separate sub-group analysis.

3. RESULTS

3.1. Patient demographics

There were 1,188 patients in the database with an average age of 61.3 ± 35.3 years, among whom 640 patients (53.9%) were females and 548 (46.1%) were males. In terms of race, a total of 846 patients (71.2%) were white, 143 (12%) were black, 66

(5.6%) were Asian, 37 (3.1%) were Hispanic, and 24 (2.0%) belonged to other racial groups. Seventy-two patients (6.1%) did not disclose their racial information.

Of all 1,188 subjects, 1,125 subjects (94.7%) had two eye scans, one for each eye, and 63 subjects (5.3%) had a scan for one eye. As a result, a total of 2,313 eyes from 1,188 subjects were scanned. There were 1,160 scans from right eyes and 1,153 from left eyes.

3.2. Eye characteristics

Eye specific characteristics are shown in Table 1, which showed that most of the scans were associated with better than 20/40 vision (80.9%), mild glaucoma stage (55.5%), reliable visual fields (69.7%), and trace to 1+ cataracts (54.9%). Of the 1222 (52.8% of the total) eye scans from patients who had their refractive errors recorded, 1141 or 93.4% were associated with refractive errors between -6.0 D SE to $+5.0$ D SE while the remaining 81 or 6.6% were associated with refractive error worse than -6.0 D SE or $+5.0$ D SE. Of the 1222 eye scans from patients who had their refraction recorded within 3 months of the OCT scan, 1186 or 97.1% had between -3.0 to $+3.0$ D of cylinder, while the remaining 35 or 2.9% had astigmatism worse than -3.0 or $+3.0$ D of cylinder.

Of the 2313 scans that were obtained from 1188 patients, the most common diagnosis was OAG that represented 34.0% of the scans. The second most common condition was glaucoma suspect that included 18.5% of the scans. Following that, in order of descending frequency, the findings included normal (12.6%), ocular hypertension (9.6%), narrow angle glaucoma (8.0%), pediatric glaucoma (0.97%). A total of 16.3% of the scans represented findings in the “other” category including diagnoses of aphakic glaucoma, chronic angle closure glaucoma, physiologic cupping, congenital glaucoma, juvenile open angle glaucoma, mixed mechanism glaucoma, normal tension glaucoma, neovascular glaucoma, pseudoexfoliation glaucoma, pigment dispersion glaucoma, traumatic glaucoma. A small number of patients with other ophthalmic conditions that were seen on the glaucoma service were also included, such as iridocorneal endothelial syndrome, plateau iris configuration, and retinal abnormalities.

3.3. Frequency of artifacts

At least one artifact was noted in 1,070 of 2,313 eye scans (46.3%). Amongst them, 820 scans had one artifact, 196 scans had 2 different types of artifact, and 54 scans had 3 or more types of artifact. Of the 12 types of artifacts, de-centration error was the most common artifact (27.8%, Table 2). The next most common artifact was related to the presence of a PVD (14.4%, Table 2).

3.4. Bivariate analysis of patient demographics and eye characteristics and artifact frequency

Scans with at least one artifact were more likely to occur in patients with vision worse than 20/40 compared to those with vision better than 20/40, with an odds ratio of 1.98 (95% CI [1.59-2.48], $p < 0.0001$, Table 3). The presence of cataracts was also associated with an increased likelihood of artifact. The odds ratios of a scan having at least one artifact in those with trace to 1+ cataract, 2+ cataract, or an intraocular lens compared to no cataract were 1.79 (95% CI [1.32-2.42], $p = 0.0002$), 2.9 (95% CI [1.90-4.44], $p < 0.0001$), and 2.26 (95% CI [1.61-3.16], $p < 0.0001$), respectively (Table 3).

Specifically, bivariate analysis was also conducted to determine the effect of cataracts on signal strength (Type 5). There was no statistically significant association between mild (trace to 1+) cataract and increased frequency of poor signal strength, with an odds ratio of 1.26 and 95% confidence interval between 0.50 to 3.17 ($p = 0.6297$). However, having moderate cataracts (2+ or worse) and having an IOL were both associated with increased frequencies of poor signal compared to not having a cataract. The odds ratio of a scan with poor signal in those with moderate cataract compared to no cataract was 5.33 (95% CI [2.01-14.11], $p = 0.0008$). The odds ratio of poor signal in scans associated an intraocular lens compared to no cataract was 4.15 (95% CI [1.67-10.33], $p = 0.022$).

In addition, more advanced glaucoma stage was associated with a greater frequency of artifacts ($p < 0.0001$, Table 3). In particular, patients with advanced glaucoma were significantly more likely to have eye scans with at least one artifact compared to patients without glaucoma with an odds ratio of 1.70 (95% CI [1.18-2.43], $p = 0.004$, Table 3). Furthermore, normal eyes and diagnoses of glaucoma suspect or ocular hypertension were found to be associated with a decreased likelihood of artifact compared with open angle glaucoma ($p = 0.0003$, Table 3). Compared to open angle

glaucoma, patients with normal eyes had fewer scans with at least one artifact with an odds ratio of 0.55 (95% CI [0.40-0.75], $p = 0.0002$, Table 3). Also, glaucoma suspects tended to have fewer peripapillary scans with at least one artifact on their eye scans compared to patients with open angle glaucoma with an odds ratio of 0.63 (95% CI [0.48-0.83], $p = 0.011$, Table 3). Furthermore, patients with ocular hypertension also had fewer scans with artifacts compared to patients with OAG, with an odds ratio of 0.68 (95% CI [0.47-0.97], $p = 0.036$, Table 3). Meanwhile, glaucoma suspects and ocular hypertension patients did not have a significant difference in prevalence of their eye scans having at least one artifact, with an odds ratio of 1.08 (95% CI [0.73-1.60], $p = 0.704$, Table 3).

The other patient factors, including age, sex, race, refractive error, astigmatism, and visual field reliability were not associated with a significant increase or decrease in the frequency of artifacts (Table 3).

3.5. Multivariate analysis of patient demographics and eye characteristics and artifact frequency

The correlation of visual acuity and cataract grading with artifact frequency remained significant in the multivariate model. VA of worse than 20/40 was associated with increased likelihood of artifacts compared with VA better than 20/40 with odds ratio of 1.70 (95% CI [1.34-2.15], $p < 0.0001$). Cataract severity was also associated with an increased likelihood of artifacts with $p < 0.0001$. Individually, RNFL scans associated with trace to 1+ cataract, 2+ cataract, and intraocular lens have odds ratios of 1.73 (95% CI [1.28-2.34], $p = 0.0004$), 2.37 (95% CI [1.53-3.66], $p = 0.0001$), and 2.00 (95% CI [1.42-2.81], $p < 0.0001$), respectively, of having at least one artifact in SD-OCT scans compared to those with normal slit lamp findings.

4. DISCUSSION

4.1. Discussion of artifact types 1 to 8

A total of twelve types of artifacts were described in our study. Five of the artifacts were described previously by Han et al²³ and included misidentification of the anterior RNFL (type 1), incorrect segmentation of the posterior RNFL (type 2), incomplete segmentation (type 3), off-center scans (type 4), and cut edge artifacts (type 7).

A total of 8 artifacts (types 1 to 8) described were independent of patient pathology. Misidentification of the anterior and posterior RNFL and incomplete segmentation were artifacts that were consistently described and observed in multiple prior OCT studies.^{23,24,46-48} These artifacts represented algorithm failures that directly led to inaccuracies in RNFL thickness measurements. When peripapillary scans were not properly centered over the optic nerve head (type 4), this could lead to inaccurate interpretations of RNFL thickness measurements, because the RNFL is normally thinner as one moves further away from the optic nerve head. Therefore, for example, if the scanned area was further away from the optic nerve head due to de-centration, the scanned RNFL area might appear artifactually thinner compared to prior centered scans.⁴⁹⁻⁵¹ Improper centration of the peripapillary circle scan was a type of error that could potentially be eliminated by an automated process, which ideally should be integrated into future OCT imaging machines.

Although Han et al did not report any motion artifacts in their SD-OCT artifact study, we saw and described motion artifacts caused by patient movement (type 8). Even though a retinal-tracking system is integrated into the commercially available Spectralis SD-OCT machine in order to improve scan registration when there is patient movement,⁵² the tracking system does not correct for large degrees of patient movement which can still cause scan artifacts that interfere with accurate RNFL segmentation and thickness measurements. On the other hand, the mirror artifact described by Han et al²³ was not observed in our study. Although mirror artifacts are theoretically possible with RNFL scans, perhaps RNFL scans compared to macular studies are less commonly associated with mirror artifacts.

Two other related artifacts included poor signal (type 5) and missing parts (type 6). Poor signal might lead to missing parts, and missing scan areas might be similar to the concept of “degraded scans” which was described in the study by Han et al.²³ As shown in Figure 6, segmentation in areas of missing scan data resulted in incorrect interpolation of the true RNFL borders.

Poor signal (type 5) was defined by the manufacturer as a quality score of less than 15 dB (range from 0 to 40 dB). It has been shown that both qualitative and quantitative evaluation of OCT images, such as RNFL measurements, are markedly influenced by the signal level.^{53–57} However, signal strength might not always reflect the quality of the image. For example, Figure 5 had a poor signal strength of 9 dB, but subjectively there was good visibility of the RNFL against the background. Huang et al proposed a subjective grading scheme for OCT image signal quality composed of 9 questions about the visibility of different retinal layers and the reflectivity between layers generating a total score of 0 to 9 based on the binary answers.⁵⁸ The grading scheme had good correlation with objective quantitative measurement of signal strength.⁵⁸ Since subjective assessment of image quality may be clinically relevant and can complement the machine-generated signal strength, the grading scheme by Huang et al may be adapted in the future to Spectralis scanning of the RNFL.

4.2. Discussion of artifact types 9 to 12

Four artifacts described in this study were related to ocular pathology. Asrani et al recently described 3 artifacts caused by patient ocular pathologies, including epiretinal membranes, posterior vitreous detachments, and high myopia.²⁴ Epiretinal membranes were not considered a separate category of artifacts in our study, but were included as artifacts in the category of misidentification of the anterior RNFL layer (type 1). Asrani et al²⁴ demonstrated that posterior vitreous detachments resulted in erroneously thickened RNFL measurements by Spectralis. Interestingly, in an earlier study by Aref et al with Cirrus, the presence of PVDs led to falsely thin RNFL thickness values in an area corresponding to the PVD.⁵⁹ 14.4% of the eye scans in our study contained artifacts caused by the presence of a PVD (type 9). PVDs may interfere with accurate longitudinal assessment of disease progression, because RNFL thickness values may decrease over time from the release of vitreous traction unrelated to

glaucoma progression, or because there may be inaccurate RNFL thickness assessments due to PVD-related algorithm failures.

High myopia, or longer axial lengths, can be independently associated with thinner RNFL thickness values.^{28–32} In particular, high myopia, or having longer axial lengths, has been reported to be associated with thinner RNFL values for all 4 quadrants.^{30–32} Therefore, because high myopia and glaucoma can independently cause RNFL thinning, RNFL thickness may be limited as a diagnostic tool for glaucoma in highly myopic patients. Independent of the association between RNFL thinning and high myopia, our paper specifically evaluated whether high myopia was associated with an increased prevalence of RNFL artifacts. Indeed, in a subgroup of 1222 eye scans with documented refraction within a period of 3 months before or after the scan, our evaluation of both spherical equivalent and cylinder failed to establish an association between high myopia and astigmatism with an increased prevalence of artifacts in Spectralis scans. This finding confirmed the conclusions of prior studies that RNFL thinning seen in highly myopic patients was due to physiologic changes and not due to artifactual RNFL thinning.

In addition, we hereby described for the first time three new types of artifacts related to patient ocular pathology, including peripapillary atrophy (type 10), staphyloma (type 11), and myelinated nerve fibers (type 12).

Peripapillary atrophy is thinning of the retina and retinal pigment epithelium in the region immediately surrounding the optic nerve head. The frequency and size of peripapillary atrophy has been shown to be greater in eyes with glaucoma than in normal eyes,^{60,61} and severe peripapillary atrophy has been shown to affect OCT RNFL thickness measurements.^{62,63} In our study, the presence of peripapillary atrophy, in a total of 27 RNFL scans, has been consistently associated with poor RNFL scan quality and inaccuracy of RNFL thickness measurements. Although the current scan circle diameter in OCT machines was selected to be large enough to be outside most areas of peripapillary atrophy but not too large such that the RNFL is too thin to be reliably segmented, OCT RNFL circular scans sometimes still scan over areas of peripapillary atrophy. In our study, most of the 27 scans were associated with artifactually thinner RNFL measurements. Therefore, even though the intent of the peripapillary scan circle

was to be large enough to avoid most areas of peripapillary atrophy, artifactually thinner RNFL measurements with peripapillary atrophy was sometimes unavoidable. Clinicians should use caution when interpreting Spectralis RNFL measurements in patients with peripapillary atrophy. Studies should be conducted in the future to better quantitatively assess the full effect of peripapillary atrophy on RNFL thickness measurements.

There have not been any studies done to date to evaluate the effect of staphyloma on OCT RNFL thickness measurements. Staphyloma is an ocular anomaly characterized by deep fundus excavation around the disc or posterior pole. Based on the 1 eye scan with staphyloma in our study, the pathology significantly interfered with accurate signal transmission during scanning, and significantly affected accurate RNFL segmentation. It is therefore a clinically significant artifact that clinicians should keep in mind when interpreting OCT scans.

Similarly, one patient in our study was found to have myelinated nerve fibers, which is a rare finding present in 0.3 to 0.6% of the population and are seen in 1% at postmortem examination.^{64,65} Even though myelinated nerve fibers should theoretically cause an increase in RNFL thickness, we found that myelinated nerve fibers could instead cause artifactually thin RNFL measurements due to incorrect segmentation of the RNFL borders (Figure 12). Clinicians should be aware that myelinated nerve fibers may cause artifacts in RNFL thickness measurements.

4.3. Discussion of patient characteristics associated with increased artifact rates

Next, we looked at the correlation of patient factors and eye conditions with frequency of artifact. A total of 10 patient factors and eye conditions were evaluated for correlation with artifact frequency. The patient factors which were not statistically associated with an increase in artifacts were age, sex, race, refractive error, astigmatism, and visual field reliability. On the other hand, factors associated with an increased prevalence of artifacts were worse visual acuity, more severe cataract, having a diagnosis of open angle glaucoma, and having advanced glaucoma.

Although best corrected visual acuity was used for this study, suboptimal patient vision during an eye scan may interfere with patient cooperation during the SD-OCT study and contribute to an increased prevalence of artifacts in eye scans.

Cataract was associated with an increased frequency of artifacts. As cataract

severity increased, it was more likely that the corresponding scan would contain at least one artifact. The odds ratio of artifact frequency was 1.79 in eyes with mild cataracts (i.e. trace to 1+ cataracts) compared to normal eyes. This increased to an odds ratio of 2.90 in eyes with moderate to severe cataracts (i.e. 2+ or worse cataract) compared to normal eyes. In an OCT study that compared pre- versus post-operative signal strengths in patients who had undergone cataract surgery, cataracts were found to decrease signal strength.⁶⁶ This finding is consistent with the fact that media opacities of any kind can degrade signal strength. Our data also confirmed this finding by showing that severe cataracts (2+ or worse) were associated with an increased frequency of poor signal strength (type 5). Interestingly, however, our data also showed that patients who have had cataract surgery had an increased frequency of artifacts compared to normal eyes, and this effect was related to its correlation with poor signal strength. There are possible reasons that a PCIOL may be associated with poor signal strength. It is possible that subtle associated posterior capsular opacification that is not visually significant may decrease light source transmission and affect signal strength. Another possibility is that the PCIOL per se may cause light scattering either off the front or back surface of the PCIOL, and this may degrade signal strength.

Our data also showed that patients with severe glaucoma were more likely to have RNFL scans with artifacts, while mild to moderate glaucoma patients were not. This may likely be due to the fact that glaucomatous RNFL thinning is associated with decreased RNFL reflectivity which may lead to more algorithm failures. This finding suggests that when physicians are reviewing Spectralis scans for patients with MD < -12, they should be aware of the increased occurrence of artifacts when interpreting the results.

The diagnosis of open angle glaucoma was associated with a higher prevalence of artifacts compared to normal eyes and other diagnoses such as ocular hypertension and glaucoma suspect. This may also be due to a decrease in RNFL reflectivity, making automated RNFL thickness determinations more difficult. Since patients under 18 years of age were excluded from the study, there were only 22 patients with pediatric glaucoma diagnoses but who were adults at the time their scans were obtained. The smaller number of patients in this diagnostic group probably could be the reason that

pediatric glaucoma was not significantly associated with artifacts in our study.

4.4. Study limitations

Our study had several limitations. First of all, since our study was conducted using Spectralis OCT imaging, our conclusions may not be generalizable to other SD-OCT machines. Second, this was a cross-sectional study, so we cannot comment on the causality of artifacts related to patient characteristics, but only speculate. Third, refractive error was only recorded for 52.8% of the total study population for unknown cause(s), and we cannot rule out the possibility that those who had refractive error recorded or not recorded had specific characteristics related to artifact rates. In other words, there could be confounding factors that diluted the association between refractive error and increased artifact rate if all patients' refractive error data were obtained at the time of the study.

4.5. Part I Conclusion

In conclusion, 46.3% of eye scans in a total of 2313 had at least one artifact. Of the 12 artifacts described, 4 were related to patient ocular pathology and two of them, staphyloma and myelinated nerve fibers, were described for the first time. Clinicians should look for artifacts and be aware that the two most common types of OCT RNFL artifacts are de-centration, with a total frequency of 27.8%, and PVD-associated errors, with a frequency of 14.4%. Also, before making therapeutic decisions based on RNFL thickness measurements, clinicians should note if the patient has any conditions that may be associated with more OCT artifacts or may affect RNFL thickness interpretations, such as the following: 1) de-centered RNFL scan, 2) PVD, 3) visual acuity less than 20/40, 4) moderate to severe cataracts, 5) past cataract surgery, 6) advanced glaucoma stage, 7) open angle glaucoma, and 8) peripapillary atrophy. Ideally, computer algorithms should allow for manual correction of algorithm errors to avoid inaccurate diagnostic information.

Part II

Diagnostic Capability of Retinal Volume for Diagnosis of Glaucoma Using Spectralis Optical Coherence Tomography Volume Scans

5. METHODS

5.1. Participants and examinations

A retrospective cross-sectional review was conducted with approval from the Massachusetts Eye and Ear Infirmary (MEEI) Institutional Review Board. All participants were recruited from the Glaucoma Service at the MEEI between January 1, 2009 and July 31, 2014, as part of the SIG (Spectral Domain OCT in Glaucoma) study. Informed consent was obtained from all subjects with adherence to the tenets of the Declaration of Helsinki and the Health Insurance Portability and Accountability Act.

Details of the study methods have been described elsewhere.⁴⁰ Briefly, all subjects underwent a complete eye examination by a glaucoma fellowship-trained ophthalmologist (T.C.C). Patients were included if they fulfilled all of the inclusion criteria: 1) a spherical equivalent between -5.0 and +5.0 diopters, 2) a best-corrected visual acuity of 20/40 or better, 3) reliable visual field (VF) with 33% or less fixation losses, 20% or less false positive results, and 20% or less false-negative results. Exclusion criteria were: 1) discernible anterior segment dysgenesis, 2) corneal scarring or opacities, 3) severe non-proliferative or proliferative diabetic retinopathy, 4) VF loss attributable to a non-glaucoma condition, 5) a dilated pupil diameter of less than 2 mm. Patients were diagnosed with OAG if they had characteristic changes of the optic nerve head (ONH) with corresponding VF defects and by ophthalmologist (T.C.C)'s clinical judgment.⁶⁷ As suggested by the manufacturer, scans with signal strength of less than 15 dB (range, 0–40) were excluded from the analysis. This study included patients with primary OAG, pigmentary, pseudoexfoliation and normal tension glaucoma. Normal subjects were those with normal examinations and confirmed by T.C.C.⁶⁸ Only the scans of OAG and normal subjects were analyzed. If both eyes were eligible, one eye was selected randomly.

5.2. Spectralis OCT peripapillary retinal volume scan

After pupillary dilation, all SD-OCT volume scan imaging was performed by the Spectralis OCT machine (HRA/Spectralis software version 5.4.8.0). Details were described previously.^{11,40,69} Each volumetric dataset consisted of 193 B-scans.

Analyses of the volume scans were performed using an in-house MATLAB program (MathWorks, Inc., Natick, MA). Four annuli were created: circumpapillary

annulus 1 (CA1) was bounded by 2.5 and 3.5 mm diameter circles (Figure 13A), CA2 by 3 and 4 mm (Figure 13B), CA3 by 3.5 and 4.5 mm (Figure 13C), and CA4 by 4 and 5 mm (Figure 13D). The MATLAB program centered the circular grids on the optic nerve (Figure 14).

Despite using a high-density 20 x 20 degree scan area, larger annuli sometimes exceeded the scanned regions, and they were excluded by the MATLAB program. Each annulus was divided into four 90-degree quadrants: superior [S], temporal [T], inferior [I], and nasal [N]. The superior and inferior quadrants were further divided into four octants/sectors: superior-temporal [ST], superior-nasal [SN], inferior-temporal [IT], inferior-nasal [IN] (Figure 15). The software automatically segmented the inner limiting membrane and retinal pigment epithelium (RPE)/Bruch's membrane complex (Figure 16). Topography of the retinal layers was shown by the color map (Figure 17). All B-scans were checked for algorithm errors. Mean retinal volume, determined by the software algorithm, was recorded for overall RV (360 degrees), each RV quadrant, and 4 octants (see Figure 15) for all 4 annuli sizes.

The average RNFL thickness values were recorded from the Spectralis printouts for the overall RNFL (360 degrees), each quadrant, and 4 octants or sectors (ST, SN, IT and IN, Figure 15).

5.3. Evaluation of artifacts on individual B-scans

Anterior segmentation error was defined as algorithm failure or incorrect segmentation of the ILM (Figure 18, red line, yellow arrow). Posterior segmentation error occurred when there was RPE/Bruch's membrane complex misidentification (Figure 19, blue line, yellow arrows). Missing scan occurred when part of the scan was missing or when a portion of the RNFL across its entire thickness was completely black or had a poor signal-to-noise ratio (Figure 20).²³ Cut edge artifacts were identified in cases of abrupt lateral edge truncation of the retina (Figure 21). Mirror artifact occurred when the retina was inverted and/or a ghost image was created from an out-of-register image (Figure 22). It was described previously by Han and Jaffe in Spectralis OCT imaging.²³

5.4. Statistical analysis

Demographics of normal and OAG subjects were compared using chi-squared tests or non-paired two-tailed Student's t-tests. Using the clinical diagnosis (OAG vs. normal) as the reference standard, diagnostic test characteristics, including sensitivity, specificity, positive and negative predictive values, and positive and negative likelihood ratios, for RV for all of the quadrants and octants of CA1 to CA4 were calculated using the cutoff value of RV that gave maximal Youden index (J), or [Sensitivity + Specificity – 1]. The same diagnostic test analyses were repeated for RNFL thickness. The area under the receiver operating characteristic (AUROC) curves for the RV parameters were compared with RNFL thickness parameters for the global, quadrant, and octant regions for all 4 RV annuli sizes and for the 1 RNFL circle size. Differences were considered significant at $p < 0.05$. To quantify the artifact rates, the number of scans with at least one artifact was divided by the total number of B-scans, which included 193 B-scans for each patient's SD-OCT volume scan. All statistical analyses were performed using R version 3.3.2 [R Core Team (2016)]. R: A language and environment for statistical computing. R Foundation for Statistical Computing, Vienna, Austria). All results are stated as means \pm standard deviation unless otherwise stated.

6. RESULTS

6.1. Patient demographics and scans

Of the 180 study subjects, 67 had normal eyes and 113 had OAG. Mean age was 62.6 years \pm 15.4 years, and 41.7% (75/180) were male. OAG patients were older than normal subjects by 13.7 years ($p < 0.0001$) and had worse visual field performance ($p < 0.0001$, Table 4).

A larger annulus size was associated with a higher percentage of regions outside the 20 x 20 scan area. Specifically, zero of a total of 180 scans from CA1, 3 scans (1.7%) from CA2, 10 scans (5.5%) from CA3, and 13 scans (7.2%) from CA4 were excluded.

6.2. RV diagnostic capability

OAG patients had lower RV values compared to normal patients for global, quadrants, and octants across four annuli ($p < 0.0001$ for all, Table 5). AUROC values

for RV of all annuli, quadrants and octants were consistently above 0.8 (Table 6). Inferior quadrant RV demonstrated the highest AUROC curve values (0.964) compared to global RV and other individual quadrant or octant RV values in their respective annuli (Table 6). The highest AUROC values were those associated with inferior RV of CA1 and CA2 (0.964 and 0.955, respectively, Table 6) and with inferior, IT, and global RNFL thickness (0.966, 0.965, and 0.959, respectively, Table 6).

Looking more closely at the regions with the highest AUROC curves, a cutoff value of 90.5 microns for inferior quadrant of RNFL thickness correctly predicted 103 out of 113 OAG cases (91.1% sensitivity), and a normal diagnosis in 65 out of 67 cases (97.0% specificity, Table 7). A cutoff value of 0.381 mm³ for CA1's inferior RV correctly predicted OAG in 106 out of 113 cases (93.8% sensitivity), and a normal diagnosis in 62 out of 67 cases (92.5% specificity, Table 7).

6.3. RV Pair-wise comparisons across four annuli

In pair-wise comparisons, AUROC for global CA1 was significantly higher than that of CA2, CA4 ($p = 0.042, 0.024$, respectively, Table 8), and AUROC for global CA3 was significantly higher than that of CA4 ($p = 0.035$, Table 8). AUROC globally was otherwise not significantly different among other pair-wise comparisons between RV annuli and between RV and RNFL thickness.

In inferior and superior quadrant and octant analyses, the annuli closer to the optic disc (i.e. CA1, CA2) consistently had better diagnostic performance in the inferior quadrants, IT and IN octants compared to annuli farther away from the optic disc (i.e. CA3 and CA4, Table 8). For example, CA1 had a higher AUROC value in the inferior quadrant compared to CA2, CA3, CA4 ($p = 0.032, 0.036, 0.028$, respectively), in the IT octant compared to CA2, CA3, CA4 ($p = 0.0089, 0.0067, 0.0051$, respectively), and in the IN octant compared to CA2, CA3, CA4 ($p = 0.0069, 0.0051, 0.0001$, respectively). Similar patterns were observed when comparing inferior quadrants and octants of CA2 with those of CA3, CA4, although not all were statistically significant (Table 8). On the other hand, AUROC of superior quadrants of all 4 annuli were not significantly different when compared pair-wise ($p > 0.05$).

In the temporal and nasal quadrant analyses, the annuli closer to the optic disc (CA1, CA2) consistently had better diagnostic performance in the nasal quadrants,

compared to annuli farther away (CA3 and CA4, Table 8). There was no significant difference in the temporal quadrants of all 4 annuli in pair-wise comparisons.

6.4. Pair-wise comparisons between 3D RV and 2D RNFL thickness measurements

Looking at RNFL thickness measurements, the best 2D RNFL thickness AUROC values for diagnosing OAG were those associated with the inferior and IT octant RNFL measurements (0.966 and 0.965, Table 6). In pair-wise comparisons with RV measurements, inferior quadrant of RNFL thickness had similar diagnostic capability compared to inferior quadrants of RV across its 4 annuli ($p > 0.05$, Table 8). On the other hand, IT octant of RNFL had better diagnostic capability compared to IT octant for RV of CA2 ($p = 0.042$), CA3 ($p = 0.015$), CA4 ($p = 0.0080$), but not significantly different from that of CA1 ($p = 0.187$). In addition, global RNFL thickness also had higher AUROC compared to that of RV of CA2 ($p = 0.0273$), CA3 ($p = 0.030$) and CA4 ($p = 0.015$), but similar to RV of CA1 ($p = 0.0675$). Otherwise, RNFL thickness and RV of all annuli had similar diagnostic performance in all other individual quadrants and octants ($p > 0.05$, Table 8).

6.5. Artifacts in 3D volume scans

Among all patients' scans, or 34,740 B-scans in total with 193 scans for each patient, a total of 2,071 scans (6.0%) had at least one artifact (Table 9). Among them, 2.5% (852/34,740) were anterior segmentation errors (Figure 18, red line, yellow arrow), and 1.5% (521/34,740) were posterior (RPE/Bruch's membrane) segmentation errors (Figure 19, blue line, yellow arrows). Missing part artifact was present among 0.4% (153/34,740) of scans (Figure 20); cut edge artifact was present among 1.9% (651/34,740) of scans (Figure 21); and finally mirror artifact, present among 0.08% (28/34,740) of B-scans (Figure 22). No de-centration errors were identified. In contrast, in the same set of 180 patients, 2D RNFL scans had an overall artifact rate of 32.2% (58/180). Among them, 5.6% (10/180) were anterior segmentation errors (Figure 1, white arrow), and 22.2% (40/180) were posterior (RNFL layer) segmentation errors (Figure 2, yellow arrow), and 9.4% (17/180) were de-centration artifacts (Figure 4). No cut edge or mirror artifacts were seen among this set of RNFL scans.

When comparing RV versus RNFL, RV had a significantly lower artifact rate per B-scan compared to RNFL scans ($p < 0.0001$, Table 9). RV also had significantly lower artifact rates in the 3 individual artifact rate categories that were compared, including anterior segmentation error, posterior segmentation error, and missing part artifact ($p < 0.0001$ for all, Table 9). Individual artifact rate break-down by normal versus OAG, and their comparisons can also be found in Table 9.

7. DISCUSSION

7.1. Discussion of annular size specification

In this study, we specifically chose annuli with inner diameters from 2.5 mm to outer diameters of 5 mm with 0.5 mm increments. Previously, our group investigated the diagnostic capability of peripapillary RT and RV, by centering the ETDRS circular grid around the ONH.^{40,43} In these two studies, ETDRS circular grid and its set dimensions (diameters of 1, 2, 3 mm; 1, 2.22, 3.45 mm; and 1, 3, 6 mm) were used since it was already built into the Heidelberg system for macular imaging. We found that peripapillary RT and RV measurements had excellent diagnostic capability, comparable to, if not better than, that of RNFL thickness measurements in glaucoma. As a result of these promising data, our group, developed software to measure peripapillary retinal volume using a new set of circumpapillary annuli, whose inner and outer diameters could be varied to any diameter. While selecting for the appropriate annular sizes, we took into account data from our previous studies that 1) RT and RV measurements from annuli of smaller diameter, such as those bounded by ETDRS diameter circles of 2, 3 mm, had better diagnostic accuracy compared to measurements from larger annuli, such as those bounded by ETDRS diameter circles of 3, 6 mm, 2) annulus bounded by diameters of 2, 3 mm and 2.22 and 3.45 mm were least affected by peripapillary atrophy (PPA), 3) as much as 23.7% of the scans fell out of the 6 x 6 mm scanned region for the largest annulus bounded by diameters 3 and 6 mm.¹⁷ As a result, in this study, we chose annuli with inner diameters from 2.5 mm to outer diameters of 5 mm, with 0.5 mm increments to maximize diagnostic accuracy and minimize the effects of peripapillary atrophy. In addition, only 7.2% of the annuli fell outside of the 6 mm x 6 mm scanned area for our largest annuli CA4, bounded by circles of diameters 4 and 5 mm.

7.2. Discussion of RV diagnostic capability

Although SD-OCT machines can acquire 3D information, much of the current glaucoma software captures information two-dimensionally, i.e. thickness (z axis) and area (x and y axes). Therefore, the full diagnostic potential of SD-OCT has not been fully realized. Compared to RT, RV inherently contains information across the entire surface area of the retina in all dimensions simultaneously, such as reflected in our three-dimensional map of the retinal tissue distribution (Figure 17). This map more closely reflects the structure of the retina in all its dimensions, and may therefore, provide a more accurate assessment of the full extent of a retinal defect. This is particularly valuable in glaucoma diagnosis and treatment where focal changes of even small magnitudes could affect clinical assessment and management.

The annulus with the highest global RV diagnostic performance was that closest to the ONH, namely CA1 (global CA1 AUOC 0.937, Tables 6 to 8). This is consistent with the observation that the closer one is to the disc margin, the higher the proportion of RNFL to total RV. The RNFL is the retinal layer that is preferentially affected in glaucoma.⁷⁰ An RV annulus closer to the optic nerve therefore is more sensitive to glaucomatous changes in the RNFL. In addition, total retinal volume decreases with increased distance from the ONH, so measuring retinal volume at a place where it is thicker allows a higher sensitivity to subtle RV changes compared to where it's thinner with an annulus farther away from the optic disc, such as CA4.⁷¹

Among individual RV quadrants and octants, the inferior quadrants for all 4 annuli sizes demonstrated the best diagnostic capability (0.945 to 0.964, Table 6). Best diagnostic ability was for the smallest size annuli (inferior CA1, 0.964, Table 6) which was similar to the AUROC curve value for inferior RNFL thickness (0.966, Table 6, $p = 0.793$). For both RV and RNFL thickness measurements, Table 6 also shows that the best diagnostic ability for distinguishing normal from glaucoma patients was for the inferior, superior, inferior temporal, and global regions, with the inferior quadrant being consistently better than the superior quadrant. This is consistent with the pattern observed previously in RNFL studies, specifically that the inferior quadrant of RNFL conferred the best diagnostic performance in detection of glaucoma using OCT.^{6,26-28} This consistency is reassuring in that the anatomical patterns of change, which are

captured in the RNFL thickness measurements between glaucoma versus normal patients, are also detected in RV measurements.

Table 7 further showed that the inferior quadrants were the most sensitive, or in other words, had the least false negatives, compared to other regions of RNFL and RV. This finding is consistent with the observation that in glaucoma, while thinning of the neuroretinal rim occurs in all sectors of the optic disc, there is a preference for the inferior pole that tend to be affected the most and before other regions.⁷⁶⁻⁷⁹ Since retinal volume is the volume of retinal tissues that feeds into the corresponding neuroretinal rim, we would expect inferior retinal volume quadrant to be the most sensitive indicator of glaucoma.

On the other hand, Table 7 also showed that global and temporal quadrants were the most specific, or had the least false positives, compared to other regions of RNFL and RV. This is again consistent with known glaucomatous progression that the thinning of inferior and superior RNFL tends to precede that of nasal or temporal RNFL thinning.⁷⁹ In addition, the excellent specificities in the nasal and temporal quadrants in this study may also be owing to the fact that 3D volume scans have good sampling of these regions, which may be affected by a high density of blood vessels and have thinner RNFL values compared to superior and inferior regions.⁸⁰ Recently, several studies that assessed 3D volume parameters demonstrated superior diagnostic capability in the nasal and temporal regions compared to traditional RNFL thickness measurements.^{36,37}

Table 8 showed pair-wise comparison patterns among RV measurements. Annuli closer to the optic nerve (CA1, CA2) were consistently found to have better diagnostic performance in the inferior quadrants as well as the IT and IN octants compared to annuli farther from ONH (CA3, CA4, Table 8). One study, using a 3.46 mm-diameter circle scan, showed that inferior RNFL defects tend to be narrower than superior defects among OAG patients with visual field defects.⁸¹ It was thought that the increased concentration of RNFL tissue inferiorly was related to the less supportive nature of lamina cribrosa in the same area with larger single pore sizes.^{79,82,83} Our results were consistent with their findings albeit measured in RV: CA1, which was the only annulus in our study that fell completely within the 3.46 diameter circle, was better at capturing the entirety of the narrower, more concentrated inferior defects that fell within a small area.

An analogous pattern can be observed in the nasal and temporal quadrants, in that annuli closer to the ONH (CA1, CA2) consistently had better diagnostic performance in the nasal quadrants compared to annuli farther away (CA3 and CA4, Table 8). One study showed that a steeper slope of the nasal peripapillary area is one of the earliest changes in glaucomatous eyes.⁸⁴ Therefore, one likely explanation for this pattern is that since there is a higher proportion of RNFL to total RV when closer to the disc margin, measurements of this thicker structure among annuli closer to ONH, such as CA1 and CA2, is less susceptible to slope variations in the nasal areas compared to annuli farther away from the ONH, such as CA3 and CA4.

7.3. Comparison between RNFL and RV diagnostic capability

When comparing the diagnostic capability of RV with RNFL (Table 8), diagnostic performance of CA1, or the annulus with the highest AUROC curve, was similar to that of RNFL thickness across most quadrants and octants (superior quadrant, $p = 0.574$; temporal quadrant, $p = 0.489$; inferior quadrant, $p = 0.793$; nasal quadrant, $p = 0.832$); and the diagnostic performance of the inferior quadrant, i.e. the quadrant with the highest AUROC curves across all four annuli, was similar to that of inferior quadrant of RNFL thickness (CA1, $p = 0.793$; CA2, $p = 0.333$; CA3, $p = 0.153$; CA4, $p = 0.162$, Table 8). In short, RV and RNFL had similar diagnostic performance when using the best annulus, i.e. CA1, or best quadrant, i.e. inferior quadrant, across all four annuli in this study. RV, therefore, had similar, but non-superior diagnostic capability compared to RNFL using an annular grid of diameters of 2.5 and 3.5 mm.

These comparison results were consistent with our group's prior study that evaluated diagnostic capability of RV measurements by centering ETDRS circular grid over ONH. This prior study found similar diagnostic capability between RV and RNFL using annular sizes of diameters of 2, 3 mm and 2.22, 3.45 mm.⁴³

7.4. 3D retinal volume artifact types and artifact rates

Our study showed that RV scans had significantly fewer artifacts compared to 2D RNFL scans in the same patient population (Table 9). Our software automatically eliminated one of the most common types of RNFL thickness artifacts, the de-centration artifact, which occurred in 9.4% of 2D RNFL scans in this study (Table 9) and in as much as 27.8% of RNFL thickness scans in a large study of over 2,000 2D RNFL

scans.⁸⁵ In addition, RV measurements had significantly fewer algorithm segmentation errors compared to RNFL thickness scans (Table 9). Most notably, while posterior segmentation errors were present in 22.2% of RNFL scans, which was the most common type of 2D RNFL artifact in this study, only 1.5% of B-scans in the volume studies had posterior segmentation errors ($p < 0.0001$, Table 9). This major difference is most likely related to the loss of RNFL reflectivity in glaucomatous eyes, making it difficult for algorithms to distinguish the posterior RNFL border from the underlying structures.⁴¹ On the other hand, there is no evidence in the literature to suggest that glaucoma causes a loss of reflectivity in the RPE/Bruch membrane complex, which is the posterior border of RV. Indeed, the difference between posterior segmentation errors of RNFL thickness versus RV was most prominent among OAG patients (27.4% vs. 1.2%, $p < 0.0001$, Table 9). Other possible factors that account for this difference include better computer software and better scan quality with current volume scans, which would also significantly decrease posterior segmentation artifacts among normal patients (13.4% vs. 1.6%, $p < 0.0001$, Table 9).

OCT artifacts are known to cause clinically significant measurement errors.²³ Recently, Mansberger and associates showed that automated segmentation by OCT without manual refinement led to lower global RNFL thickness values and over-classification of glaucoma.⁸⁶ As much as 23.7% of borderline classifications, or yellow coding on OCT, became normal after manual refinement of segmentation. These occurrences, along with red disease (false positives) and green disease (false negatives), can be minimized by better imaging scan protocols, such as with OCT volume scans; algorithm refinement, such as with automated centration; better segmentation algorithms, such as those customized for glaucoma; and better diagnostic parameters, such as RV.

7.5. Study limitations

Our study had several limitations. First of all, we applied very strict inclusion and exclusion criteria while recruiting subjects for the study. The cutoff values were derived to maximize the AUROC curve values. In the clinical setting, cutoff values are generally derived from a large normative database of patients with diverse backgrounds and eye pathologies. Our AUROC values, therefore, are expected to be significantly lower in the

clinical setting with a much more diverse patient population with many eye pathologies related or unrelated to glaucoma. Moreover, the OAG patients were significantly older than normal subjects. While this was consistent with the fact that glaucoma incidence increases with age⁸⁷⁻⁸⁹ and is reflective of the patient population clinicians encounter every day, we could not rule out the possibility that the differences we detected may partly be age-related and independent of glaucomatous changes. However, future studies on the normal age-related loss for 3D parameters need to be done. Our study was also limited by the fact that all our OAG patients had VF defects with a mean MD of less than -12 dB. Therefore, our findings were not generalizable to all glaucoma patients.

In addition, even though we reviewed 193 B-scans for all 180 patients, the strict inclusion and exclusion criteria of the study excluded certain patient pathologies that would incur certain types of artifacts on scans. As a result, our characterizations of artifacts in 3D volume scan may not be the most comprehensive.

7.6. Part II conclusion

Our study showed that 3D peripapillary retinal volume has similar diagnostic capability for OAG compared to the widely used 2D RNFL thickness measurement. Retinal volume measurements were however less affected by artifacts compared to RNFL thickness scans, making it a more reliable imaging parameter for diagnostic purposes. Best RV regions and annuli sizes included the inferior quadrant and the CA1 annulus, bounded by circular diameters of 2.5 mm and 3.5 mm.

8. FUTURE DIRECTIONS

8.1. Evaluate patient characteristic associations with groups of artifacts

In Part I of the thesis, we evaluated associations between patient characteristics and individual 12 types of artifacts. These 12 types of artifacts, however, can be briefly divided into 3 major groups: algorithm failure (such as anterior and posterior segmentation errors and incomplete segmentation error), capturing failure (such as de-centration, poor signal, missing parts, cut edge and motion artifact), and patient pathology induced errors (such as PVD, PPA, staphyloma, MNFL associated errors). In

the future, studies can be conducted to evaluate if there is any significant associations between patient characteristics and these major groups of artifacts. This will help to indicate exactly what part of the current OCT imaging technique is most lacking, i.e. algorithm vs. capturing techniques.

8.2. Artifact evaluation for 3D volume scans

Even though Part II of the study systemically evaluated artifacts in individual B-scans, given that the purpose of the study was to evaluate diagnostic capability, strict inclusion and exclusion criteria were employed that prevented a more general patient population as studied in Part I. Future studies should be conducted to include a more general patient population, with all kinds of eye pathologies, to be evaluated for eye-pathology related artifacts similar to what was done in Part I of the thesis.

In addition, future studies could be conducted to evaluate patient and eye characteristics that are associated with a higher prevalence of artifact in 3D volume scans. This would serve to inform clinicians in evaluating the data generated by volume scans and software algorithm.

8.3. Retinal volume's diagnostic capability in pre-perimetric glaucoma

Since structural defects were known to precede functional VF loss, future studies that aim to study the diagnostic value of RV in pre-perimetric glaucoma would be valuable. Since a visual field loss is still a critical component of establishing a diagnosis of glaucoma, retrospective studies could be a reasonable starting point to evaluate past SD-OCT volume scans among patients who later went on to develop perimetric glaucoma.

8.4. Peripapillary atrophy's effects on retinal volume's diagnostic capability

We did not evaluate the effects of peripapillary atrophy, a common eye condition, on the diagnostic capability of retinal volume. However, it is an important consideration when choosing the appropriate annular size for retinal volume measurements. In this study, instead of evaluating it quantitatively, we relied on the experience and data generated in prior studies^{40,43} to inform our choice of annular size. Future studies should be conducted to assess how peripapillary atrophy could affect retinal volume's diagnostic capability across the annular sizes used in this study.

9. SUMMARY

In this two-part thesis, we sought to 1) evaluate artifacts in RNFL thickness measurements by SD-OCT, one of the most important limitations of the most commonly used diagnostic imaging modality in glaucoma, and 2) evaluate the diagnostic capability of retinal volume, a new OCT measurement, using 3D OCT volume scans for glaucoma diagnosis.

In Part I of this thesis, we not only described 12 different artifact types and their rates, but also demonstrated that certain patient and eye characteristics were associated with a higher prevalence of artifacts. These results promised to better inform clinicians both common artifacts to assess for and patient characteristics to note when interpreting results from RNFL thickness scan results before making therapeutic decisions.

In Part II of this thesis, we evaluated peripapillary retinal volume measurements from Spectralis volume scans using a new set of annular sizes (diameters of 2.5, 3.5 mm; 3, 4 mm; 3.5, 4.5 mm; 4, 5 mm) as a diagnostic test for OAG. We also determined the best circumpapillary annuli sizes for glaucoma diagnosis and demonstrated that the diagnostic capability of RV using annulus of diameters of 2.5 and 3.5 mm was equal to that of the traditional 2D RNFL thickness parameters but with lower artifact rates for diagnosing perimetric OAG.

REFERENCES

1. Kingman S. Glaucoma is second leading cause of blindness globally. *Bull World Health Organ.* 2004;82(11):887-888. doi:/S0042-96862004001100019.
2. Tham Y-C, Li X, Wong TY, Quigley HA, Aung T, Cheng C-Y. Global Prevalence of Glaucoma and Projections of Glaucoma Burden through 2040: A Systematic Review and Meta-Analysis. *Ophthalmology.* 2014;121(11):2081-2090. doi:10.1016/j.ophtha.2014.05.013.
3. Kapetanakis VV, Chan MPY, Foster PJ, Cook DG, Owen CG, Rudnicka AR. Global variations and time trends in the prevalence of primary open angle glaucoma (POAG): a systematic review and meta-analysis. *Br J Ophthalmol.* 2016;100(1):86-93. doi:10.1136/bjophthalmol-2015-307223.
4. Quigley HA, Broman AT. The number of people with glaucoma worldwide in 2010 and 2020. *Br J Ophthalmol.* 2006;90(3):262-267. doi:10.1136/bjo.2005.081224.
5. Friedman DS, O'Colmain BJ, Muñoz B, et al. Prevalence of age-related macular degeneration in the United States. *Arch Ophthalmol.* 2004;122(4):564-572. doi:10.1001/archopht.122.4.564.
6. Coleman AL. Glaucoma. *Lancet Lond Engl.* 1999;354(9192):1803-1810. doi:10.1016/S0140-6736(99)04240-3.
7. Friedman NJ, Kaiser PK, Trattler B. *Review of Ophthalmology.* Philadelphia: Elsevier Saunders; 2005.
8. Kerrigan-Baumrind LA, Quigley HA, Pease ME, Kerrigan DF, Mitchell RS. Number of ganglion cells in glaucoma eyes compared with threshold visual field tests in the same persons. *Invest Ophthalmol Vis Sci.* 2000;41(3):741-748.
9. Maier PC, Funk J, Schwarzer G, Antes G, Falck-Ytter YT. Treatment of ocular hypertension and open angle glaucoma: meta-analysis of randomised controlled trials. *BMJ.* 2005;331(7509):134. doi:10.1136/bmj.38506.594977.E0.
10. Huang D, Swanson EA, Lin CP, et al. Optical coherence tomography. *Science.* 1991;254(5035):1178-1181.
11. Chen TC, Cense B, Pierce MC, et al. Spectral domain optical coherence tomography: ultra-high speed, ultra-high resolution ophthalmic imaging. *Arch Ophthalmol.* 2005;123(12):1715-1720. doi:10.1001/archopht.123.12.1715.
12. Blumenthal EZ, Weinreb RN. Assessment of the retinal nerve fiber layer in clinical trials of glaucoma neuroprotection. *Surv Ophthalmol.* 2001;45 Suppl 3:S305-312-334.

13. Quigley HA, Addicks EM, Green WR. Optic nerve damage in human glaucoma. III. Quantitative correlation of nerve fiber loss and visual field defect in glaucoma, ischemic neuropathy, papilledema, and toxic neuropathy. *Arch Ophthalmol*. 1982;100(1):135-146.
14. Quigley HA, Dunkelberger GR, Green WR. Retinal ganglion cell atrophy correlated with automated perimetry in human eyes with glaucoma. *Am J Ophthalmol*. 1989;107(5):453-464.
15. Mwanza J-C, Oakley JD, Budenz DL, Anderson DR, Cirrus Optical Coherence Tomography Normative Database Study Group. Ability of cirrus HD-OCT optic nerve head parameters to discriminate normal from glaucomatous eyes. *Ophthalmology*. 2011;118(2):241-248.e1. doi:10.1016/j.ophtha.2010.06.036.
16. Sung KR, Na JH, Lee Y. Glaucoma diagnostic capabilities of optic nerve head parameters as determined by Cirrus HD optical coherence tomography. *J Glaucoma*. 2012;21(7):498-504. doi:10.1097/IJG.0b013e318220dbb7.
17. Kotowski J, Folio LS, Wollstein G, et al. Glaucoma discrimination of segmented cirrus spectral domain optical coherence tomography (SD-OCT) macular scans. *Br J Ophthalmol*. 2012;96(11):1420-1425. doi:10.1136/bjophthalmol-2011-301021.
18. Jeoung JW, Choi YJ, Park KH, Kim DM. Macular ganglion cell imaging study: glaucoma diagnostic accuracy of spectral-domain optical coherence tomography. *Invest Ophthalmol Vis Sci*. 2013;54(7):4422-4429. doi:10.1167/iovs.12-11273.
19. Lisboa R, Paranhos A, Weinreb RN, Zangwill LM, Leite MT, Medeiros FA. Comparison of different spectral domain OCT scanning protocols for diagnosing preperimetric glaucoma. *Invest Ophthalmol Vis Sci*. 2013;54(5):3417-3425. doi:10.1167/iovs.13-11676.
20. Ervin A-M, Boland MV, Myrowitz EH, et al. *Screening for Glaucoma: Comparative Effectiveness*. Rockville (MD): Agency for Healthcare Research and Quality (US); 2012. <http://www.ncbi.nlm.nih.gov/books/NBK95371/>. Accessed January 19, 2017.
21. Mylonas G, Ahlers C, Malamos P, et al. Comparison of retinal thickness measurements and segmentation performance of four different spectral and time domain OCT devices in neovascular age-related macular degeneration. *Br J Ophthalmol*. 2009;93(11):1453-1460. doi:10.1136/bjo.2008.153643.
22. Ho J, Sull AC, Vuong LN, et al. Assessment of artifacts and reproducibility across spectral- and time-domain optical coherence tomography devices. *Ophthalmology*. 2009;116(10):1960-1970. doi:10.1016/j.ophtha.2009.03.034.
23. Han IC, Jaffe GJ. Evaluation of artifacts associated with macular spectral-domain optical coherence tomography. *Ophthalmology*. 2010;117(6):1177-1189.e4. doi:10.1016/j.ophtha.2009.10.029.

24. Asrani S, Essaid L, Alder BD, Santiago-Turla C. Artifacts in Spectral-Domain Optical Coherence Tomography Measurements in Glaucoma. *JAMA Ophthalmol.* 2014;132(4):396. doi:10.1001/jamaophthalmol.2013.7974.
25. Gurses-Ozden R, Ishikawa H, Hoh ST, et al. Increasing sampling density improves reproducibility of optical coherence tomography measurements. *J Glaucoma.* 1999;8(4):238-241.
26. Wu H, de Boer JF, Chen TC. Reproducibility of retinal nerve fiber layer thickness measurements using spectral domain optical coherence tomography. *J Glaucoma.* 2011;20(8):470-476. doi:10.1097/IJG.0b013e3181f3eb64.
27. van der Schoot J, Vermeer KA, de Boer JF, Lemij HG. The effect of glaucoma on the optical attenuation coefficient of the retinal nerve fiber layer in spectral domain optical coherence tomography images. *Invest Ophthalmol Vis Sci.* 2012;53(4):2424-2430. doi:10.1167/iovs.11-8436.
28. Leung CK-S, Mohamed S, Leung KS, et al. Retinal nerve fiber layer measurements in myopia: An optical coherence tomography study. *Invest Ophthalmol Vis Sci.* 2006;47(12):5171-5176. doi:10.1167/iovs.06-0545.
29. Rauscher FM, Sekhon N, Feuer WJ, Budenz DL. Myopia affects retinal nerve fiber layer measurements as determined by optical coherence tomography. *J Glaucoma.* 2009;18(7):501-505. doi:10.1097/IJG.0b013e318193c2be.
30. Mohammad Salih PA-K. Evaluation of peripapillary retinal nerve fiber layer thickness in myopic eyes by spectral-domain optical coherence tomography. *J Glaucoma.* 2012;21(1):41-44. doi:10.1097/IJG.0b013e3181fc8053.
31. Zhao J-J, Zhuang W-J, Yang X-Q, Li S-S, Xiang W. Peripapillary retinal nerve fiber layer thickness distribution in Chinese with myopia measured by 3D-optical coherence tomography. *Int J Ophthalmol.* 2013;6(5):626-631. doi:10.3980/j.issn.2222-3959.2013.05.13.
32. Savini G, Barboni P, Parisi V, Carbonelli M. The influence of axial length on retinal nerve fibre layer thickness and optic-disc size measurements by spectral-domain OCT. *Br J Ophthalmol.* 2012;96(1):57-61. doi:10.1136/bjo.2010.196782.
33. Lee KYC, Tomidokoro A, Sakata R, et al. Cross-sectional anatomic configurations of peripapillary atrophy evaluated with spectral domain-optical coherence tomography. *Invest Ophthalmol Vis Sci.* 2010;51(2):666-671. doi:10.1167/iovs.09-3663.
34. Kim SY, Park H-YL, Park CK. The effects of peripapillary atrophy on the diagnostic ability of Stratus and Cirrus OCT in the analysis of optic nerve head parameters and disc size. *Invest Ophthalmol Vis Sci.* 2012;53(8):4475-4484. doi:10.1167/iovs.12-9682.

35. Leal-Fonseca M, Rebolleda G, Oblanca N, Moreno-Montañes J, Muñoz-Negrete FJ. A comparison of false positives in retinal nerve fiber layer, optic nerve head and macular ganglion cell-inner plexiform layer from two spectral-domain optical coherence tomography devices. *Graefes Arch Clin Exp Ophthalmol Albrecht Von Graefes Arch Für Klin Exp Ophthalmol*. 2014;252(2):321-330. doi:10.1007/s00417-013-2529-7.
36. Tsikata E, Lee R, Shieh E, et al. Comprehensive Three-Dimensional Analysis of the Neuroretinal Rim in Glaucoma Using High-Density Spectral-Domain Optical Coherence Tomography Volume Scans. *Invest Ophthalmol Vis Sci*. 2016;57(13):5498-5508. doi:10.1167/iovs.16-19802.
37. Shieh E, Lee R, Que C, et al. Diagnostic Performance of a Novel Three-Dimensional Neuroretinal Rim Parameter for Glaucoma Using High-Density Volume Scans. *Am J Ophthalmol*. 2016;169:168-178. doi:10.1016/j.ajo.2016.06.028.
38. Chen TC. Spectral domain optical coherence tomography in glaucoma: qualitative and quantitative analysis of the optic nerve head and retinal nerve fiber layer (an AOS thesis). *Trans Am Ophthalmol Soc*. 2009;107:254-281.
39. Povazay B, Hofer B, Hermann B, et al. Minimum distance mapping using three-dimensional optical coherence tomography for glaucoma diagnosis. *J Biomed Opt*. 2007;12(4):41204. doi:10.1117/1.2773736.
40. Simavli H, Que CJ, Akduman M, et al. Diagnostic Capability of Peripapillary Retinal Thickness in Glaucoma Using 3D Volume Scans. *Am J Ophthalmol*. December 2014. doi:10.1016/j.ajo.2014.12.004.
41. Tah V, Keane PA, Esposti SD, et al. Repeatability of retinal thickness and volume metrics in neovascular age-related macular degeneration using the Topcon 3DOCT-1000. *Indian J Ophthalmol*. 2014;62(9):941-948. doi:10.4103/0301-4738.143936.
42. Andreoli MT, Lim JI. Optical coherence tomography retinal thickness and volume measurements in X-linked retinoschisis. *Am J Ophthalmol*. 2014;158(3):567-573.e2. doi:10.1016/j.ajo.2014.05.028.
43. Simavli H, Poon LY-C, Que CJ, et al. Diagnostic Capability of Peripapillary Retinal Volume Measurements in Glaucoma. *J Glaucoma*. January 2017. doi:10.1097/IJG.0000000000000621.
44. Alasil T, Wang K, Keane PA, et al. Analysis of Normal Retinal Nerve Fiber Layer Thickness by Age, Sex, and Race Using Spectral Domain Optical Coherence Tomography. *J Glaucoma*. April 2012. doi:10.1097/IJG.0b013e318255bb4a.
45. Heidelberg Engineering. Spectralis HRA + OCT User Guide. Software Version 5.3.

46. Ghazi NG, Kirk T, Allam S, Yan G. Quantification of error in optical coherence tomography central macular thickness measurement in wet age-related macular degeneration. *Am J Ophthalmol.* 2009;148(1):90-96.e2. doi:10.1016/j.ajo.2009.02.017.
47. Keane PA, Mand PS, Liakopoulos S, Walsh AC, Sadda SR. Accuracy of retinal thickness measurements obtained with Cirrus optical coherence tomography. *Br J Ophthalmol.* 2009;93(11):1461-1467. doi:10.1136/bjo.2008.155846.
48. Krebs I, Hagen S, Brannath W, et al. Repeatability and reproducibility of retinal thickness measurements by optical coherence tomography in age-related macular degeneration. *Ophthalmology.* 2010;117(8):1577-1584. doi:10.1016/j.ophtha.2010.04.032.
49. Vizzeri G, Bowd C, Medeiros FA, Weinreb RN, Zangwill LM. Effect of improper scan alignment on retinal nerve fiber layer thickness measurements using Stratus optical coherence tomograph. *J Glaucoma.* 2008;17(5):341-349. doi:10.1097/IJG.0b013e31815c3aeb.
50. Yoo C, Suh IH, Kim YY. The influence of eccentric scanning of optical coherence tomography on retinal nerve fiber layer analysis in normal subjects. *Ophthalmol J Int Ophthalmol Int J Ophthalmol Z Für Augenheilkd.* 2009;223(5):326-332. doi:10.1159/000221836.
51. Cheung CYL, Yiu CKF, Weinreb RN, et al. Effects of scan circle displacement in optical coherence tomography retinal nerve fibre layer thickness measurement: a RNFL modelling study. *Eye Lond Engl.* 2009;23(6):1436-1441. doi:10.1038/eye.2008.258.
52. Hammer DX, Ferguson RD, Magill JC, et al. Active retinal tracker for clinical optical coherence tomography systems. *J Biomed Opt.* 2005;10(2):24038. doi:10.1117/1.1896967.
53. Wu Z, Vazeen M, Varma R, et al. Factors associated with variability in retinal nerve fiber layer thickness measurements obtained by optical coherence tomography. *Ophthalmology.* 2007;114(8):1505-1512. doi:10.1016/j.ophtha.2006.10.061.
54. Barkana Y, Burgansky-Eliash Z, Gerber Y, et al. Inter-device variability of the Stratus optical coherence tomography. *Am J Ophthalmol.* 2009;147(2):260-266. doi:10.1016/j.ajo.2008.08.008.
55. Sung KR, Wollstein G, Schuman JS, et al. Scan quality effect on glaucoma discrimination by glaucoma imaging devices. *Br J Ophthalmol.* 2009;93(12):1580-1584. doi:10.1136/bjo.2008.152223.
56. Huang J, Liu X, Wu Z, Sadda S. Image quality affects macular and retinal nerve fiber layer thickness measurements on fourier-domain optical coherence

- tomography. *Ophthalmic Surg Lasers Imaging Off J Int Soc Imaging Eye*. 2011;42(3):216-221. doi:10.3928/15428877-20110324-01.
57. Balasubramanian M, Bowd C, Vizzeri G, Weinreb RN, Zangwill LM. Effect of image quality on tissue thickness measurements obtained with spectral domain-optical coherence tomography. *Opt Express*. 2009;17(5):4019-4036.
 58. Huang Y, Gangaputra S, Lee KE, et al. Signal quality assessment of retinal optical coherence tomography images. *Invest Ophthalmol Vis Sci*. 2012;53(4):2133-2141. doi:10.1167/iovs.11-8755.
 59. Aref AA, Budenz DL. Spectral domain optical coherence tomography in the diagnosis and management of glaucoma. *Ophthalmic Surg Lasers Imaging Off J Int Soc Imaging Eye*. 2010;41 Suppl:S15-27. doi:10.3928/15428877-20101031-01.
 60. Jonas JB, Nguyen XN, Gusek GC, Naumann GO. Parapapillary chorioretinal atrophy in normal and glaucoma eyes. I. Morphometric data. *Invest Ophthalmol Vis Sci*. 1989;30(5):908-918.
 61. Jonas JB, Naumann GO. Parapapillary chorioretinal atrophy in normal and glaucoma eyes. II. Correlations. *Invest Ophthalmol Vis Sci*. 1989;30(5):919-926.
 62. Lai E, Wollstein G, Price LL, et al. Optical coherence tomography disc assessment in optic nerves with peripapillary atrophy. *Ophthalmic Surg Lasers Imaging Off J Int Soc Imaging Eye*. 2003;34(6):498-504.
 63. Doshi A, Kreidl KO, Lombardi L, Sakamoto DK, Singh K. Nonprogressive glaucomatous cupping and visual field abnormalities in young Chinese males. *Ophthalmology*. 2007;114(3):472-479. doi:10.1016/j.ophtha.2006.07.036.
 64. Kodama T, Hayasaka S, Setogawa T. Myelinated retinal nerve fibers: prevalence, location and effect on visual acuity. *Ophthalmol J Int Ophthalmol Int J Ophthalmol Z Für Augenheilkd*. 1990;200(2):77-83.
 65. Straatsma BR, Foos RY, Heckenlively JR, Taylor GN. Myelinated retinal nerve fibers. *Am J Ophthalmol*. 1981;91(1):25-38.
 66. Mwanza JC, Bhorade AM, Sekhon N, et al. Effect of cataract and its removal on signal strength and peripapillary retinal nerve fiber layer optical coherence tomography measurements. *J Glaucoma*. 2011;20(1):37-43. doi:10.1097/IJG.0b013e3181ccb93b.
 67. Wu H, de Boer JF, Chen TC. Diagnostic capability of spectral-domain optical coherence tomography for glaucoma. *Am J Ophthalmol*. 2012;153(5):815-826.e2. doi:10.1016/j.ajo.2011.09.032.
 68. Gordon MO, Kass MA. The Ocular Hypertension Treatment Study: design and baseline description of the participants. *Arch Ophthalmol*. 1999;117(5):573-583.

69. Cense B, Nassif N, Chen T, et al. Ultrahigh-resolution high-speed retinal imaging using spectral-domain optical coherence tomography. *Opt Express*. 2004;12(11):2435-2447.
70. Varma R, Skaf M, Barron E. Retinal nerve fiber layer thickness in normal human eyes. *Ophthalmology*. 1996;103(12):2114-2119.
71. Schuman JS, Pedut-Kloizman T, Hertzmark E, et al. Reproducibility of nerve fiber layer thickness measurements using optical coherence tomography. *Ophthalmology*. 1996;103(11):1889-1898.
72. Nakatani Y, Higashide T, Ohkubo S, Takeda H, Sugiyama K. Evaluation of macular thickness and peripapillary retinal nerve fiber layer thickness for detection of early glaucoma using spectral domain optical coherence tomography. *J Glaucoma*. 2011;20(4):252-259. doi:10.1097/IJG.0b013e3181e079ed.
73. Schulze A, Lamparter J, Pfeiffer N, Berisha F, Schmidtman I, Hoffmann EM. Diagnostic ability of retinal ganglion cell complex, retinal nerve fiber layer, and optic nerve head measurements by Fourier-domain optical coherence tomography. *Graefes Arch Clin Exp Ophthalmol Albrecht Von Graefes Arch Für Klin Exp Ophthalmol*. 2011;249(7):1039-1045. doi:10.1007/s00417-010-1585-5.
74. Na JH, Sung KR, Baek S, Sun JH, Lee Y. Macular and retinal nerve fiber layer thickness: which is more helpful in the diagnosis of glaucoma? *Invest Ophthalmol Vis Sci*. 2011;52(11):8094-8101. doi:10.1167/iovs.11-7833.
75. Rao HL, Zangwill LM, Weinreb RN, Sample PA, Alencar LM, Medeiros FA. Comparison of different spectral domain optical coherence tomography scanning areas for glaucoma diagnosis. *Ophthalmology*. 2010;117(9):1692-1699, 1699.e1. doi:10.1016/j.ophtha.2010.01.031.
76. Tuulonen A, Airaksinen PJ. Initial glaucomatous optic disk and retinal nerve fiber layer abnormalities and their progression. *Am J Ophthalmol*. 1991;111(4):485-490.
77. Quigley HA. Early detection of glaucomatous damage. II. Changes in the appearance of the optic disk. *Surv Ophthalmol*. 1985;30(2):111, 117-126.
78. Pederson JE, Anderson DR. The mode of progressive disc cupping in ocular hypertension and glaucoma. *Arch Ophthalmol Chic Ill 1960*. 1980;98(3):490-495.
79. Jonas JB, Fernández MC, Stürmer J. Pattern of glaucomatous neuroretinal rim loss. *Ophthalmology*. 1993;100(1):63-68.
80. Jonas JB, Gusek GC, Naumann GO. Optic disc, cup and neuroretinal rim size, configuration and correlations in normal eyes. *Invest Ophthalmol Vis Sci*. 1988;29(7):1151-1158.

81. Choi JA, Park H-YL, Jung K-I, Hong KH, Park CK. Difference in the properties of retinal nerve fiber layer defect between superior and inferior visual field loss in glaucoma. *Invest Ophthalmol Vis Sci*. 2013;54(10):6982-6990. doi:10.1167/iovs.13-12344.
82. Jonas JB, Mardin CY, Schlötzer-Schrehardt U, Naumann GO. Morphometry of the human lamina cribrosa surface. *Invest Ophthalmol Vis Sci*. 1991;32(2):401-405.
83. Hood DC, Raza AS, de Moraes CGV, Johnson CA, Liebmann JM, Ritch R. The Nature of Macular Damage in Glaucoma as Revealed by Averaging Optical Coherence Tomography Data. *Transl Vis Sci Technol*. 2012;1(1):3. doi:10.1167/tvst.1.1.3.
84. Dong J, Chihara E. Slope analysis of the optic disc in eyes with ocular hypertension and early normal tension glaucoma by confocal scanning laser ophthalmoscope. *Br J Ophthalmol*. 2001;85(1):56-62.
85. Liu Y, Simavli H, Que C, et al. Patient Characteristics Associated with Artifacts in Spectralis Optical Coherence Tomography Imaging of the Retinal Nerve Fiber Layer in Glaucoma. *Am J Ophthalmol*. December 2014. doi:10.1016/j.ajo.2014.12.006.
86. Mansberger SL, Menda SA, Fortune BA, Gardiner SK, Demirel S. Automated Segmentation Errors When Using Optical Coherence Tomography to Measure Retinal Nerve Fiber Layer Thickness in Glaucoma. *Am J Ophthalmol*. 2017;174:1-8. doi:10.1016/j.ajo.2016.10.020.
87. Chauhan BC, Mikelberg FS, Balaszi AG, et al. Canadian Glaucoma Study: 2. risk factors for the progression of open-angle glaucoma. *Arch Ophthalmol Chic Ill 1960*. 2008;126(8):1030-1036. doi:10.1001/archophth.126.8.1030.
88. Leske MC, Heijl A, Hyman L, et al. Predictors of long-term progression in the early manifest glaucoma trial. *Ophthalmology*. 2007;114(11):1965-1972. doi:10.1016/j.ophtha.2007.03.016.
89. Mukesh BN, McCarty CA, Rait JL, Taylor HR. Five-year incidence of open-angle glaucoma: the visual impairment project. *Ophthalmology*. 2002;109(6):1047-1051.

TABLES AND FIGURES

Table 1. Eye characteristics of the study population of 1188 patients who had a total of 2313 Spectralis optical coherence tomography scans of the retinal nerve fiber layer

Eye characteristics	Number of scans	Percentage (%)
Visual acuity		
Better than 20/40	1871	80.9
Worse than 20/40	437	18.9
None recorded	5	0.2
Refractive error		
-6.0 SE to +5.0 SE	1141	49.3
Worse than -6.0 SE or +5.0 SE	81	3.5
None recorded	1091	47.2
Astigmatism		
-3.0 to +3.0 cylinder	1186	51.3
Worse than -3.0 or +3.0 cylinder	36	1.56
None recorded	1091	47.2
Glaucoma stage		
Normal	266	11.5
Mild	1283	55.5
Moderate	341	14.7
Severe	273	11.8
None recorded	15	6.5
Visual field reliability		
Reliable	1611	69.7
Unreliable	526	22.7
None recorded	176	7.6
Cataract		
No cataract	324	14.4
Trace or 1+	1271	54.9
2+ or worse	199	8.6
IOL	487	21.1
None recorded	22	1.0

IOL = intraocular lens; SE = spherical equivalent

Table 2. Prevalence of the 12 types of artifacts in a total of 2,313 scans from 1,188 patients who underwent Spectralis optical coherence tomography imaging of the retinal nerve fiber layer.

Artifact Number	Artifact	Number of scans	Percentage of scans (%)
1	Anterior RNFL misidentification	73	3.16
2	Posterior RNFL misidentification	177	7.7
3	Incomplete segmentation	14	0.6
4	De-centration	644	27.8
5	Poor signal	118	5.10
6	Missing parts	35	1.51
7	Cut edge	4	0.17
8	Motion artifact	5	0.22
9	PVD-associated error	332	14.4
10	PPA-associated error	27	1.2
11	Staphyloma-associated error	1	0.04
12	MNFL-associated error	1	0.04

RNFL = retinal nerve fiber layer; PVD = posterior vitreous detachment; PPA = peripapillary atrophy; MNFL = myelinated nerve fiber layer; OR = odds ratio

Table 3. Bivariate analyses to determine if specific patient factors are associated with an increased frequency of artifacts in 2,313 scans from 1,188 patients who underwent Spectralis optical coherence tomography imaging of the retinal nerve fiber layer.

Factors	OR (95%CI)	P value
Age	1.01 (0.99-1.02)	0.076
Sex (Female vs. Male)	1.12 (0.92-1.35)	0.27
Race (Black vs. White)	0.90 (0.66-1.21)	0.65
(Asian vs. White)	1.09 (0.70-1.69)	0.47
(Hispanic vs. White)	0.89 (0.50-1.56)	0.70
(Others vs. White)	0.59 (0.26-1.34)	0.67
VA (Worse than 20/40 vs. Better than 20/40)	1.98 (1.59-2.48)	0.21
^a Spherical refractive errors (Worse than -6.0 SE or worse than +5.0 SE vs. within -6.0 SE to +5.0 SE)	1.16 (0.69-1.95)	<0.0001
^a Cylindrical refractive errors (Worse than -3.0 or worse than +3.0 cylinder vs. within -3.0 to 3.0cylinder)	1.98 (0.93-4.21)	0.5848
Visual field reliability (Reliable vs. Unreliable)	1.05 (0.86-1.30)	0.0762
Cataract (Trace 1+ vs. No cataract)	1.79 (1.32-2.42)	0.62
(2+ or worse vs. No cataract)	2.90 (1.90-4.44)	<0.0001
(IOL vs. No cataract)	2.26 (1.61-3.16)	<0.0001
Stage of Glaucoma (Mild vs. Normal)	0.86 (0.65-1.13)	<0.0001
(Moderate vs. Normal)	1.10 (0.79-1.54)	0.2667
(Advanced vs. Normal)	1.70 (1.18-2.43)	0.5678
Diagnosis of glaucoma (Narrow angle vs. Open angle)	1.19 (0.81-1.76)	0.0040
(OHTN vs. Open angle)	0.68 (0.47-0.97)	0.0003
(No glaucoma or normal vs. Open angle)	0.55 (0.40-0.75)	0.38
(Pediatric childhood vs. Open angle)	0.76 (0.25-2.32)	0.036
(Glaucoma suspect vs. Open angle)	0.63 (0.48-0.83)	0.0002
(Other vs. Open angle)	0.73 (0.54-0.97)	0.63
(OHTN vs. Glaucoma suspect)	1.08 (0.73-1.60)	0.0011
		0.030
		0.704

VA = visual acuity; SE = spherical equivalent; IOL = intraocular lens; OHTN = ocular hypertension; OR = odds ratio

^a Analyzed using a subgroup of 1,222 eye scans with corresponding refractive errors documented.

Table 4. Demographics of the normal and open-angle glaucoma study population

	Normal	OAG	P value^a
Number of eyes	67	113	
Number of right eyes/left eyes	31/36	63/50	0.26
Sex (male/female)	20/47	66/47	0.013
Mean age (years) ± SD	54.0 ± 16.5	67.9 ± 12.1	<0.0001
Refractive error (D)			
Spherical equivalent ± SD	-0.46 ± 1.86	-0.67 ± 1.84	0.49
Visual field (dB)			
Mean deviation	-1.40 ± 1.90	-12.5 ± 7.73	<0.0001
Pattern standard deviation	1.50 ± 0.28	8.51 ± 3.41	<0.0001

D = diopter; dB = decibel; OAG = open-angle glaucoma; SD = standard deviation

^a P values obtained from chi-squared tests for categorical variables and two-tailed Student t-tests for continuous variables.

Table 5. Mean retinal volume and retinal nerve fiber layer thickness measurements for normal and open-angle glaucoma patients using four circumpapillary annuli

	Global	Superior	Temporal	Inferior	Nasal	Superior-temporal	Superior-nasal	Interior-temporal	Inferior-nasal
CA1 (mm³)^a									
Normal	1.58	0.42	0.38	0.42	0.36	0.21	0.21	0.21	0.21
OAG	1.34	0.35	0.34	0.33	0.32	0.18	0.17	0.17	0.17
CA2 (mm³)^a									
Normal	1.76	0.46	0.44	0.46	0.40	0.23	0.23	0.23	0.23
OAG	1.52	0.39	0.39	0.37	0.36	0.20	0.19	0.19	0.19
CA3 (mm³)^a									
Normal	1.94	0.50	0.50	0.50	0.44	0.25	0.25	0.25	0.25
OAG	1.70	0.43	0.45	0.41	0.41	0.22	0.21	0.21	0.21
CA4 (mm³)^a									
Normal	2.12	0.54	0.56	0.54	0.48	0.27	0.27	0.27	0.27
OAG	1.88	0.47	0.51	0.45	0.44	0.24	0.23	0.23	0.23
RNFL (mm³)^a									
Normal	93.8	113	69.5	122	70.5	127	98.6	137	107
OAG	58.0	69.2	50.0	63.0	49.5	75.0	63.3	63.5	62.6

CA1 = smallest circumpapillary annulus bounded by circular grids with diameters of 2.5 and 3.5 mm; CA2 = circumpapillary annulus bounded by diameters of 3 and 4 mm; CA3 = circumpapillary annulus bounded by diameters of 3.5 and 4.5 mm; CA4 = largest circumpapillary annulus bounded by diameters of 4 and 5 mm; OAG = open-angle glaucoma; RNFL = retinal nerve fiber layer

^a p < 0.0001 for all values, when comparing normal versus OAG groups.

Table 6. Area under the receiver operating characteristic curve of retinal nerve fiber layer thickness and peripapillary retinal volume for normal versus primary open angle glaucoma patients.

	AUROC (SE)				
	CA1	CA2	CA3	CA4	RNFL
Global	0.937 (0.017)	0.929 (0.019)	0.929 (0.020)	0.912 (0.023)	0.959 (0.013)
Superior	0.928 (0.019)	0.934 (0.017)	0.934 (0.017)	0.915 (0.021)	0.937 (0.017)
Temporal	0.834 (0.029)	0.830 (0.030)	0.823 (0.030)	0.816 (0.032)	0.854 (0.029)
Inferior	0.964 (0.013)	0.955 (0.015)	0.945 (0.018)	0.945 (0.018)	0.966 (0.012)
Nasal	0.837 (0.030)	0.831 (0.031)	0.823 (0.032)	0.817 (0.034)	0.829 (0.031)
ST	0.917 (0.020)	0.908 (0.022)	0.896 (0.023)	0.874 (0.026)	0.933 (0.019)
SN	0.904 (0.023)	0.899 (0.023)	0.889 (0.024)	0.863 (0.030)	0.869 (0.026)
IT	0.947 (0.017)	0.931 (0.019)	0.919 (0.021)	0.910 (0.022)	0.965 (0.013)
IN	0.950 (0.015)	0.927 (0.020)	0.904 (0.025)	0.877 (0.028)	0.905 (0.021)

AUROC = area under receiving receiver operating characteristic curve; CA1 = smallest circumpapillary annulus bounded by circular grids with diameters of 2.5 and 3.5 mm; CA2 = circumpapillary annulus bounded by diameters of 3 and 4 mm; CA3 = circumpapillary annulus bounded by diameters of 3.5 and 4.5 mm; CA4 = circumpapillary annulus by diameters of 4 and 5 mm; IN = inferior-nasal; IT = inferior-temporal; RNFL = retinal nerve fiber layer; SE = standard error; SN = superior-nasal; ST = superior-temporal.

Table 7. Diagnostic ability of retinal volume versus retinal nerve fiber layer thickness in diagnosing open-angle glaucoma

	Cutoff value (mm ³)	Sensitivity (95% CI)	Specificity (95% CI)	PPV (95% CI)	NPV (95% CI)	PLR (95% CI)	NLR (95% CI)
CA1							
Global	1.44	0.858 (0.780 - 0.917)	0.940 (0.854 - 0.984)	0.960 (0.902 - 0.989)	0.798 (0.692 - 0.880)	14.4 (5.54 - 37.3)	0.151 (0.095 - 0.238)
Superior	0.387	0.858 (0.780 - 0.917)	0.910 (0.815 - 0.966)	0.942 (0.878 - 0.978)	0.792 (0.685 - 0.876)	9.59 (4.45 - 20.6)	0.156 (0.098 - 0.246)
Temporal	0.347	0.664 (0.569 - 0.750)	0.925 (0.834 - 0.975)	0.938 (0.860 - 0.979)	0.620 (0.518 - 0.715)	8.89 (3.79 - 20.9)	0.363 (0.278 - 0.475)
Inferior	0.381	0.938 (0.877 - 0.975)	0.925 (0.834 - 0.975)	0.955 (0.898 - 0.985)	0.899 (0.802 - 0.958)	12.6 (5.40 - 29.2)	0.067 (0.033 - 0.138)
Nasal	0.342	0.805 (0.720 - 0.874)	0.791 (0.674 - 0.881)	0.867 (0.786 - 0.925)	0.707 (0.590 - 0.806)	3.85 (2.40 - 6.20)	0.246 (0.166 - 0.365)
ST	0.192	0.814 (0.730 - 0.881)	0.910 (0.815 - 0.966)	0.939 (0.872 - 0.977)	0.744 (0.636 - 0.834)	9.09 (4.22 - 19.6)	0.204 (0.138 - 0.302)
SN	0.195	0.867 (0.791 - 0.924)	0.806 (0.691 - 0.892)	0.883 (0.808 - 0.936)	0.783 (0.667 - 0.873)	4.47 (2.73 - 7.32)	0.165 (0.101 - 0.268)
IT	0.189	0.885 (0.811 - 0.937)	0.910 (0.815 - 0.966)	0.943 (0.881 - 0.979)	0.824 (0.718 - 0.903)	9.88 (4.59 - 21.3)	0.126 (0.075 - 0.212)
IN	0.187	0.867 (0.791 - 0.924)	0.925 (0.834 - 0.975)	0.952 (0.890 - 0.984)	0.805 (0.699 - 0.887)	11.6 (4.99 - 27.1)	0.143 (0.089 - 0.231)
CA2							
Global	1.62	0.855 (0.775 - 0.915)	0.940 (0.854 - 0.984)	0.959 (0.899 - 0.989)	0.798 (0.692 - 0.880)	14.3 (5.52 - 37.1)	0.155 (0.098 - 0.244)
Superior	0.431	0.856 (0.777 - 0.957)	0.896 (0.797 - 0.957)	0.931 (0.864 - 0.972)	0.790 (0.681 - 0.875)	8.19 (4.05 - 16.6)	0.161 (0.102 - 0.255)
Temporal	0.401	0.673 (0.578 - 0.758)	0.896 (0.797 - 0.957)	0.916 (0.834 - 0.965)	0.619 (0.514 - 0.715)	6.44 (3.16 - 13.1)	0.366 (0.277 - 0.482)
Inferior	0.412	0.894 (0.822 - 0.944)	0.940 (0.854 - 0.984)	0.962 (0.905 - 0.990)	0.840 (0.737 - 0.915)	15.0 (5.78 - 38.8)	0.113 (0.066 - 0.194)
Nasal	0.377	0.714 (0.621 - 0.796)	0.851 (0.743 - 0.926)	0.889 (0.805 - 0.945)	0.640 (0.532 - 0.740)	4.79 (2.67 - 8.58)	0.336 (0.246 - 0.458)
ST	0.218	0.856 (0.777 - 0.915)	0.836 (0.725 - 0.915)	0.896 (0.822 - 0.947)	0.778 (0.664 - 0.867)	5.21 (3.02 - 9.00)	0.173 (0.108 - 0.275)
SN	0.212	0.838 (0.756 - 0.901)	0.806 (0.691 - 0.892)	0.877 (0.799 - 0.933)	0.750 (0.634 - 0.845)	4.32 (2.63 - 7.08)	0.201 (0.130 - 0.312)
IT	0.206	0.876 (0.801 - 0.931)	0.910 (0.815 - 0.966)	0.943 (0.880 - 0.979)	0.813 (0.707 - 0.894)	9.78 (4.55 - 21.1)	0.136 (0.083 - 0.224)
IN	0.200	0.805 (0.720 - 0.874)	0.925 (0.834 - 0.975)	0.948 (0.883 - 0.983)	0.738 (0.631 - 0.828)	10.8 (4.62 - 25.2)	0.210 (0.144 - 0.308)
CA3							
Global	1.79	0.822 (0.737 - 0.890)	0.952 (0.867 - 0.990)	0.967 (0.907 - 0.993)	0.760 (0.650 - 0.849)	17.3 (5.70 - 52.3)	0.186 (0.124 - 0.281)
Superior	0.465	0.818 (0.733 - 0.885)	0.940 (0.854 - 0.984)	0.957 (0.895 - 0.988)	0.759 (0.653 - 0.846)	13.7 (5.28 - 35.6)	0.193 (0.130 - 0.289)
Temporal	0.459	0.673 (0.578 - 0.758)	0.866 (0.760 - 0.937)	0.894 (0.809 - 0.950)	0.611 (0.505 - 0.709)	5.01 (2.69 - 9.32)	0.378 (0.286 - 0.501)
Inferior	0.451	0.885 (0.811 - 0.937)	0.925 (0.834 - 0.975)	0.952 (0.892 - 0.984)	0.827 (0.722 - 0.904)	11.9 (5.09 - 27.6)	0.124 (0.074 - 0.208)
Nasal	0.413	0.642 (0.545 - 0.732)	0.905 (0.804 - 0.964)	0.921 (0.836 - 0.971)	0.594 (0.489 - 0.693)	6.74 (3.11 - 14.6)	0.396 (0.304 - 0.515)
ST	0.234	0.827 (0.744 - 0.910)	0.866 (0.760 - 0.937)	0.910 (0.836 - 0.950)	0.753 (0.642 - 0.849)	6.16 (3.33 - 11.1)	0.200 (0.131 - 0.289)

		- 0.893)	- 0.937)	- 0.958)	- 0.844)	11.4)	- 0.304)
SN	0.229	0.764 (0.673	0.836 (0.725	0.884 (0.802	0.683 (0.571	4.65 (2.68 -	0.283 (0.199
		- 0.839)	- 0.915)	- 0.941)	- 0.781)	8.06)	- 0.402)
IT	0.227	0.894 (0.822	0.881 (0.778	0.927 (0.861	0.831 (0.723	7.49 (3.89 -	0.121 (0.070
		- 0.944)	- 0.947)	- 0.968)	- 0.910)	14.4)	- 0.207)
IN	0.222	0.850 (0.770	0.881 (0.778	0.923 (0.854	0.776 (0.666	7.12 (3.70 -	0.171 (0.109
		- 0.910)	- 0.947)	- 0.966)	- 0.864)	13.7)	- 0.267)
CA4							
Global	1.99	0.849 (0.762	0.875 (0.759	0.923 (0.848	0.766 (0.643	6.79 (3.38 -	0.173 (0.108
		- 0.913)	- 0.948)	- 0.969)	- 0.863)	13.6)	- 0.279)
Superior	0.505	0.793 (0.703	0.917 (0.816	0.944 (0.874	0.714 (0.600	9.51 (4.09 -	0.226 (0.155
		- 0.865)	- 0.972)	- 0.982)	- 0.812)	22.1)	- 0.331)
Temporal	0.507	0.595 (0.497	0.955 (0.875	0.957 (0.878	0.587 (0.489	13.3 (4.35 -	0.424 (0.337
		- 0.687)	- 0.991)	- 0.991)	- 0.681)	40.6)	- 0.535)
Inferior	0.504	0.946 (0.886	0.866 (0.760	0.921 (0.855	0.906 (0.807	7.04 (3.83 -	0.062 (0.029
		- 0.980)	- 0.937)	- 0.963)	- 0.965)	13.0)	- 0.137)
Nasal	0.449	0.602 (0.503	0.934 (0.841	0.942 (0.858	0.570 (0.467	9.18 (3.52 -	0.426 (0.335
		- 0.695)	- 0.982)	- 0.984)	- 0.669)	24.0)	- 0.542)
ST	0.252	0.774 (0.682	0.850 (0.734	0.901 (0.821	0.680 (0.562	5.16 (2.80 -	0.266 (0.184
		- 0.849)	- 0.929)	- 0.954)	- 0.783)	9.50)	- 0.385)
SN	0.244	0.717 (0.621	0.867 (0.754	0.905 (0.821	0.634 (0.521	5.38 (2.79 -	0.327 (0.237
		- 0.800)	- 0.941)	- 0.958)	- 0.738)	10.4)	- 0.449)
IT	0.246	0.901 (0.830	0.851 (0.743	0.909 (0.839	0.838 (0.729	6.04 (3.40 -	0.117 (0.066
		- 0.950)	- 0.926)	- 0.956)	- 0.916)	10.7)	- 0.206)
IN	0.236	0.748 (0.657	0.881 (0.778	0.912 (0.834	0.678 (0.569	6.26 (3.24 -	0.287 (0.206
		- 0.825)	- 0.947)	- 0.961)	- 0.774)	12.1)	- 0.399)
RNFL							
Global	72.0	0.821 (0.738	0.970 (0.896	0.979 (0.925	0.765 (0.660	27.5 (7.01 -	0.184 (0.124
		- 0.887)	- 0.996)	- 0.997)	- 0.850)	108)	- 0.274)
Superior	88.0	0.813 (0.728	0.925 (0.834	0.948 (0.883	0.747 (0.640	10.9 (4.66 -	0.203 (0.137
		- 0.880)	- 0.975)	- 0.983)	- 0.836)	25.4)	- 0.300)
Temporal	57.5	0.759 (0.669	0.881 (0.778	0.914 (0.838	0.686 (0.577	6.36 (3.29 -	0.274 (0.195
		- 0.835)	- 0.947)	- 0.962)	- 0.782)	12.3)	- 0.385)
Inferior	90.5	0.911 (0.842	0.970 (0.896	0.981 (0.932	0.867 (0.768	30.5 (7.78 -	0.092 (0.051
		- 0.956)	- 0.996)	- 0.998)	- 0.934)	120)	- 0.167)
Nasal	67.5	0.866 (0.789	0.657 (0.531	0.808 (0.726	0.746 (0.616	2.53 (1.80 -	0.204 (0.124
		- 0.923)	- 0.769)	- 0.874)	- 0.850)	3.54)	- 0.337)
ST	108.5	0.893 (0.820	0.866 (0.760	0.917 (0.849	0.829 (0.720	6.65 (3.61 -	0.124 (0.072
		- 0.943)	- 0.937)	- 0.962)	- 0.908)	12.2)	- 0.213)
SN	69.5	0.652 (0.556	0.925 (0.834	0.936 (0.857	0.614 (0.512	8.73 (3.72 -	0.376 (0.290
		- 0.739)	- 0.975)	- 0.979)	- 0.709)	20.5)	- 0.489)
IT	109	0.946 (0.887	0.925 (0.834	0.955 (0.898	0.912 (0.818	12.7 (5.45 -	0.058 (0.027
		- 0.980)	- 0.975)	- 0.985)	- 0.967)	29.5)	- 0.127)
IN	75.5	0.741 (0.650	0.910 (0.815	0.933 (0.859	0.678 (0.571	8.28 (3.83 -	0.284 (0.206
		- 0.819)	- 0.966)	- 0.975)	- 0.773)	17.9)	- 0.393)

CA1 = smallest circumpapillary annulus bounded by circular grids with diameters of 2.5 and 3.5 mm; CA2 = circumpapillary annulus bounded by diameters of 3 and 4 mm; CA3 = circumpapillary annulus bounded by diameters of 3.5 and 4.5 mm; CA4 = circumpapillary annulus by diameters of 4 and 5 mm; CI = confidence interval; IN = inferior-nasal; IT = inferior-temporal; NLR = negative likelihood ratio; NPV = negative predictive value; OAG = open-angle glaucoma; PLR = positive likelihood ratio; PPV = positive predictive value; RNFL = retinal nerve fiber layer; SN = superior-nasal; ST = superior-temporal.

Table 8. Pair-wise comparisons of the diagnostic abilities for retinal volume and retinal nerve fiber layer thickness

	Global	Superior	Temporal	Inferior	Nasal	ST	SN	IT	IN
CA1 vs. CA2									
ΔAUROC ^a	0.0076	-0.0054	0.0042	0.0087	0.0056	0.0086	0.0052	0.0163	0.0237
P values ^b	0.042	0.341	0.530	0.032	0.146	0.345	0.495	0.0089	0.0069
CA1 vs. CA3									
ΔAUROC	0.0077	-0.0059	0.0107	0.0183	0.0131	0.0203	0.0149	0.0278	0.0461
P values	0.118	0.584	0.429	0.036	0.034	0.041	0.238	0.0067	0.0051
CA1 vs. CA4									
ΔAUROC	0.0245	0.0133	0.0180	0.0182	0.0196	0.0421	0.0411	0.0370	0.0735
P values	0.024	0.405	0.458	0.028	0.039	0.0076	0.070	0.0051	0.0001
CA2 vs. CA3									
ΔAUROC	0.0001	-0.0005	0.0065	0.0096	0.0075	0.0117	0.0097	0.0115	0.0224
P values	0.692	0.975	0.465	0.067	0.033	0.013	0.108	0.067	0.0081
CA2 vs. CA4									
ΔAUROC	0.0169	0.0187	0.0138	0.0095	0.0140	0.0335	0.0359	0.0207	0.0498
P values	0.073	0.103	0.513	0.039	0.057	0.0012	0.024	0.017	<0.0001
CA3 vs. CA4									
ΔAUROC	0.0168	0.0192	0.0073	-0.0001	0.0065	0.0218	0.0262	0.0092	0.0274
P values	0.035	0.066	0.606	0.728	0.170	0.0087	0.031	0.0057	0.0002
RNFL vs. CA1									
ΔAUROC	0.0229	0.0081	0.0205	0.0024	-	0.0165	-	0.0173	-0.0452
P values	0.0675	0.574	0.489	0.793	0.0071	0.832	0.0345	0.145	0.187
RNFL vs. CA2									
ΔAUROC	0.0305	0.0027	0.0247	0.0111	-	0.0251	-	0.0336	-0.0215
P values	0.0273	0.844	0.407	0.333	0.0015	0.877	0.0293	0.201	0.042
RNFL vs. CA3									
ΔAUROC	0.0306	0.0022	0.0312	0.0207	0.0060	0.0368	-	0.0451	0.0009
P values	0.030	0.886	0.300	0.153	0.748	0.089	0.0196	0.482	0.015
RNFL vs. CA4									
ΔAUROC	0.0474	0.0214	0.0385	0.0206	0.0125	0.0586	0.0066	0.0543	0.0283
P values	0.015	0.406	0.241	0.162	0.481	0.044	0.861	0.0080	0.319

AUROC = area under the receiver operating characteristic curve; CA1 = inner circumpapillary annulus bounded by circular grids with diameters of 2.5 and 3.5 mm; CA2 = circumpapillary annulus bounded by diameters of 3mm and 4 mm; CA3 = circumpapillary annulus 3 bounded diameters of 3.5 and 4.5 mm; CA4 = circumpapillary annulus by diameters of 4 and 5 mm; IN = inferior-nasal; IT = inferior-temporal; RNFL = retinal nerve fiber layer; SN = superior-nasal; ST = superior-temporal.

^a ΔAUROC, or difference in AUROC, is calculated by subtracting the AUROC of retinal volume of the first annulus from that of the second annulus (i.e. ΔAUROC of CA1 vs. CA2 represents AUROC of CA1 minus CA2)

^b All P values were obtained from pair-wise comparisons

Table 9. Artifact rate comparison between 3D retinal volume scans and 2D retinal nerve fiber layer thickness scans

	RV (All) N (%)	RNFL (All) N (%)	P value	RV (Normal) N (%)	RNFL (Normal) N (%)	P value	RV (OAG) N (%)	RNFL (OAG) N (%)	P value
Overall	2071 (6.0)	58 (32.2)	<0.0001	506 (3.9)	18 (26.9)	<0.0001	1565 (7.2)	40 (35.4)	<0.0001
Anterior segmentation	852 (2.45)	10 (5.6)	<0.0001	117 (0.90)	4 (6.0)	0.003	700 (3.2)	6 (5.3)	0.18
Posterior segmentation	521 (1.5)	40 (22.2)	<0.0001	203 (1.6)	9 (13.4)	<0.0001	257 (1.2)	31 (27.4)	<0.0001
De-centration	0	17 (9.4)	NA	0	8 (11.9)	NA	0	9 (8.0)	NA
Missing parts	153 (0.44)	7 (3.9)	<0.0001	20 (0.15)	2 (3.0)	0.006	127 (0.58)	5 (4.4)	0.001
Cut edge	651 (1.9)	0	NA	141 (1.1)	0	NA	468 (2.1)	0	NA
Mirror artifact	28 (0.08)	0	NA	22 (0.17)	0	NA	6 (0.027)	0	NA

NA = not available; OAG = open-angle glaucoma; RNFL = retinal nerve fiber layer; RV = retinal volume

^a All P values were obtained from comparisons using Fisher's exact test

Figure 1. Examples of type 1 and 2 artifacts in Spectralis optical coherence tomography imaging of retinal nerve fiber layer in glaucoma. A type 1 artifact is an incorrectly segmented anterior retinal nerve fiber layer (white arrow). A type 2 artifact is an incorrectly segmented posterior retinal nerve fiber layer (yellow arrow).

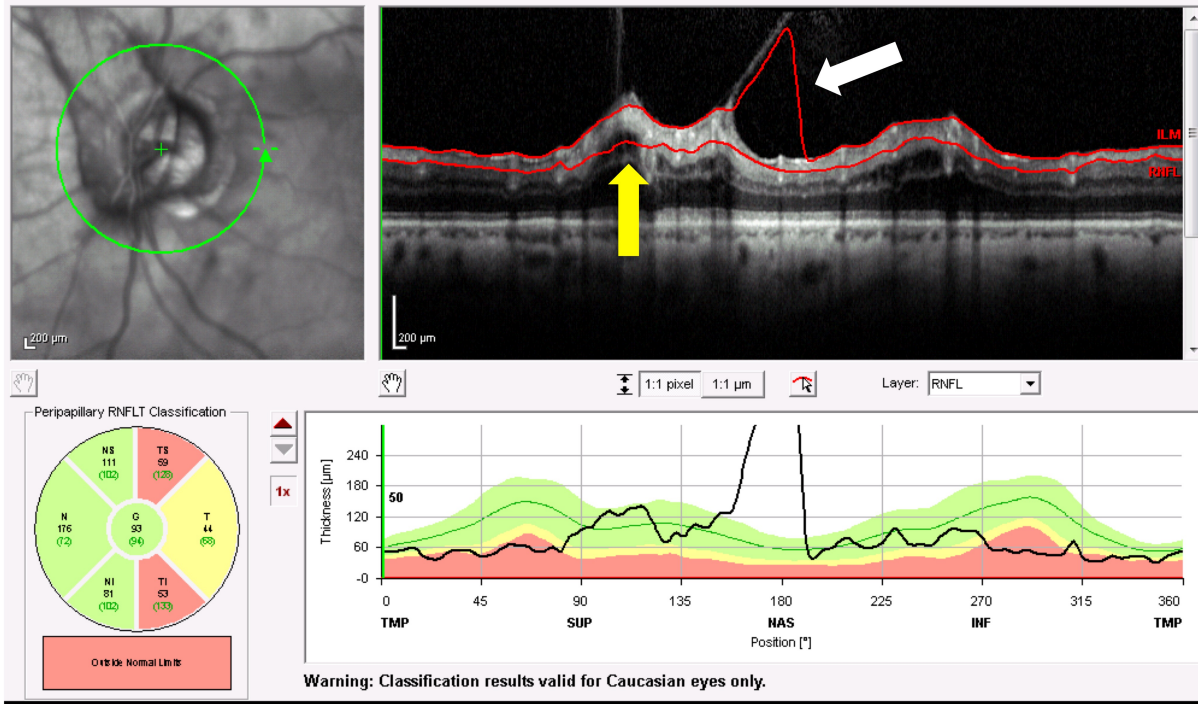


Figure 2. Example of a type 2 artifact in Spectralis optical coherence tomography imaging of retinal nerve fiber layer in glaucoma. A type 2 artifact is an incorrectly segmented posterior retinal nerve fiber layer (yellow arrow).

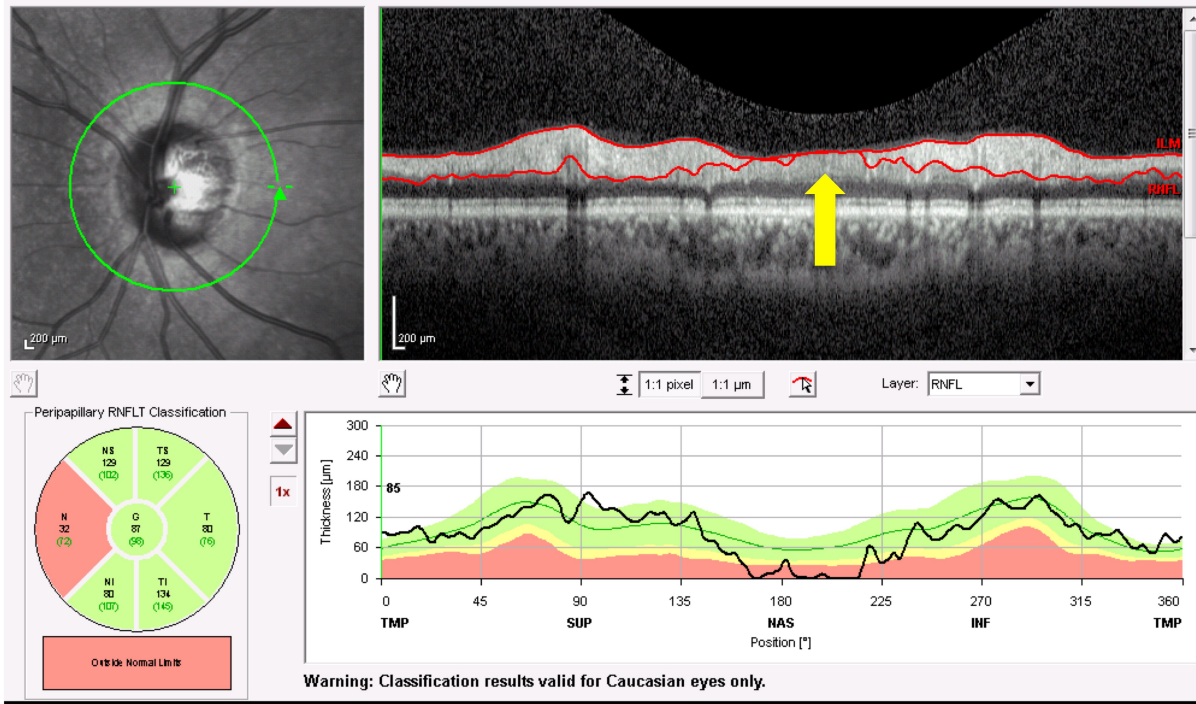


Figure 3. Example of a type 3 artifact in Spectralis optical coherence tomography imaging of retinal nerve fiber layer in glaucoma. A type 3 artifact is failure to completely segment the borders of the retinal nerve fiber layer.

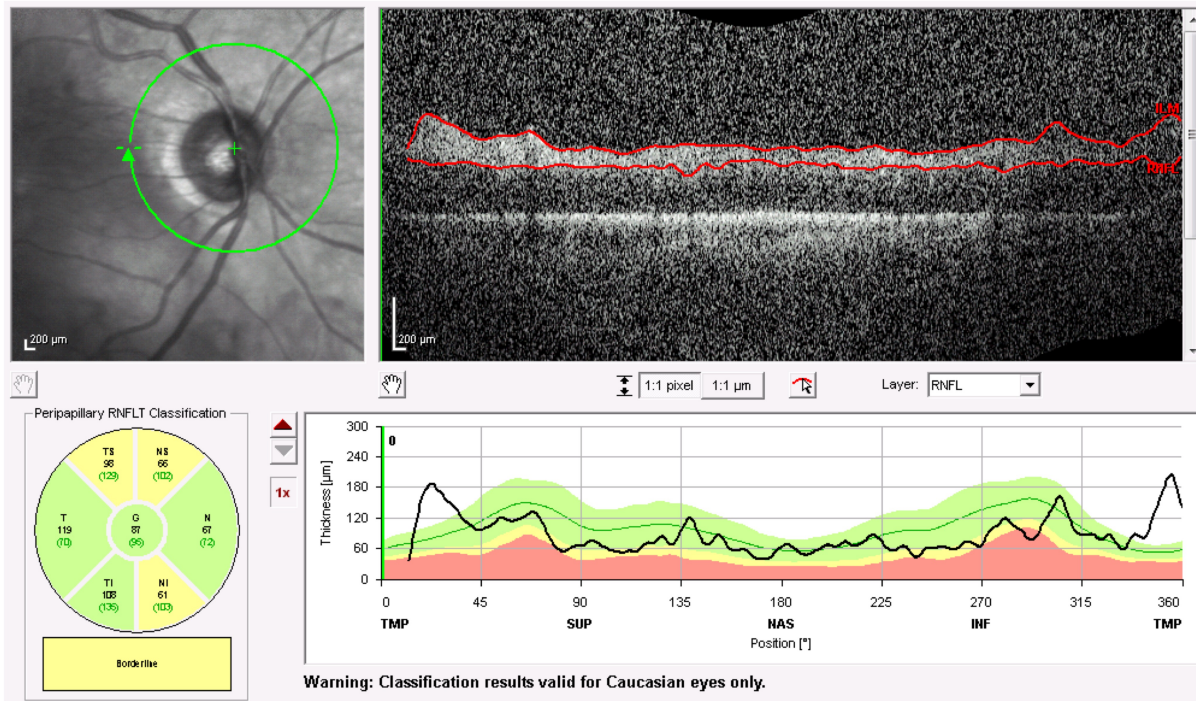


Figure 4. Example of a type 4 artifact in Spectralis optical coherence tomography imaging of retinal nerve fiber layer in glaucoma. A type 4 artifact is a de-centered scan with the center of the optic nerve head more than 10% off the center of the peripapillary circular scan.

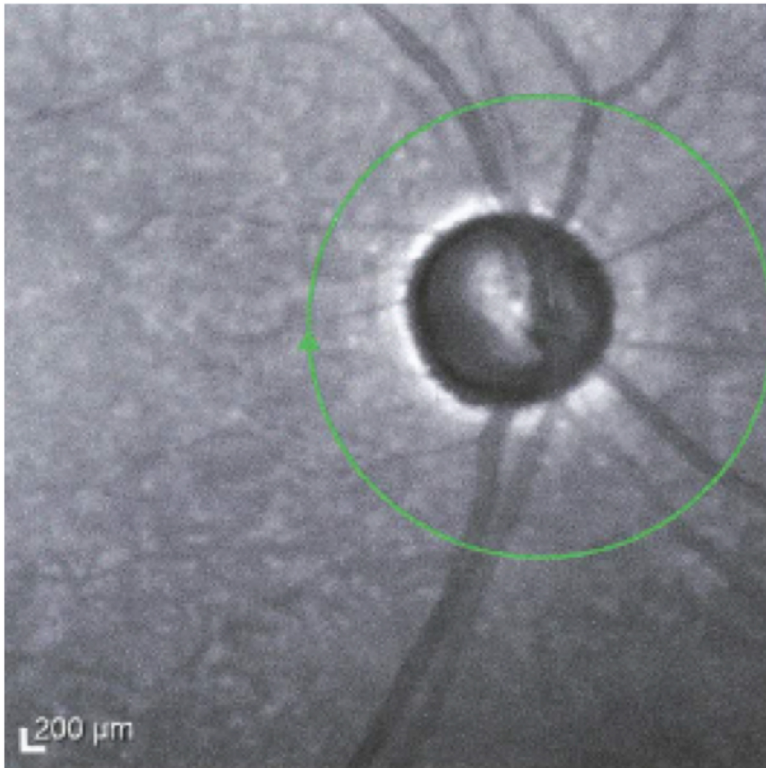


Figure 5. Example of a type 5 artifact in Spectralis optical coherence tomography imaging of retinal nerve fiber layer in glaucoma. A type 5 artifact is a poor signal scan, with quality value less than 15 (yellow arrow).

OCT ART (9) Q: 9 [HS]

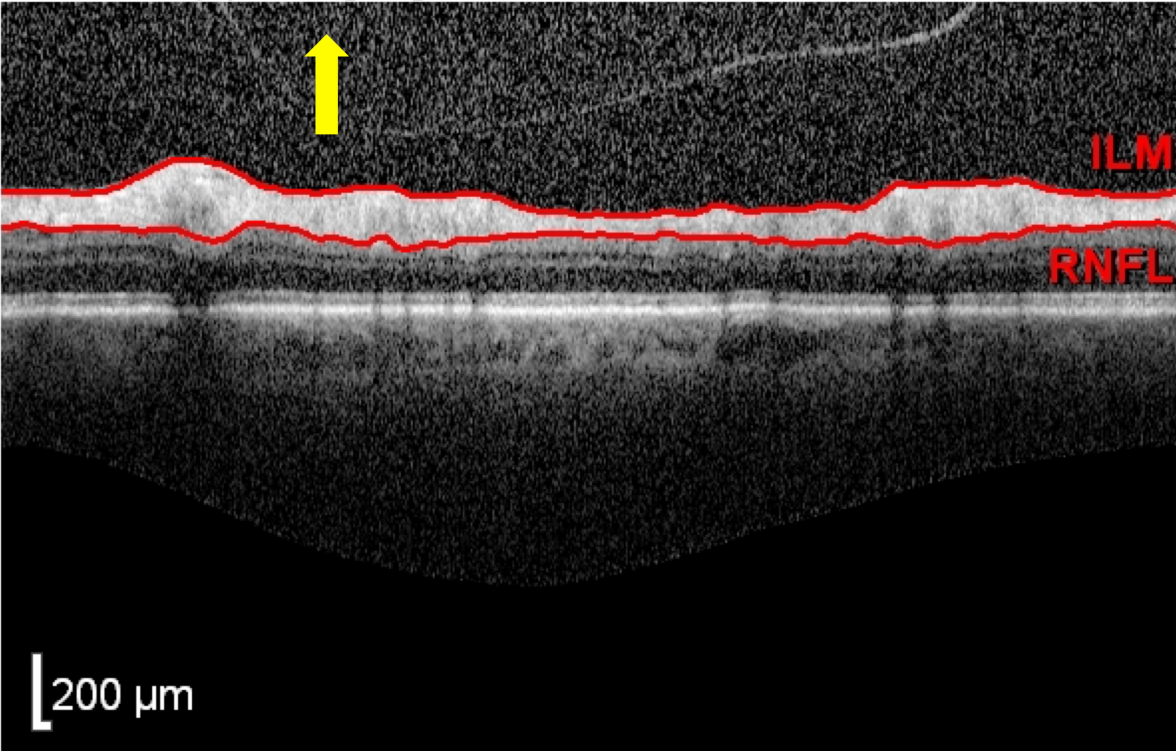


Figure 6. Example of a type 6 artifact in Spectralis optical coherence tomography imaging of retinal nerve fiber layer in glaucoma. A type 6 artifact is an image which is missing portions of the retinal nerve fiber layer (yellow arrow).

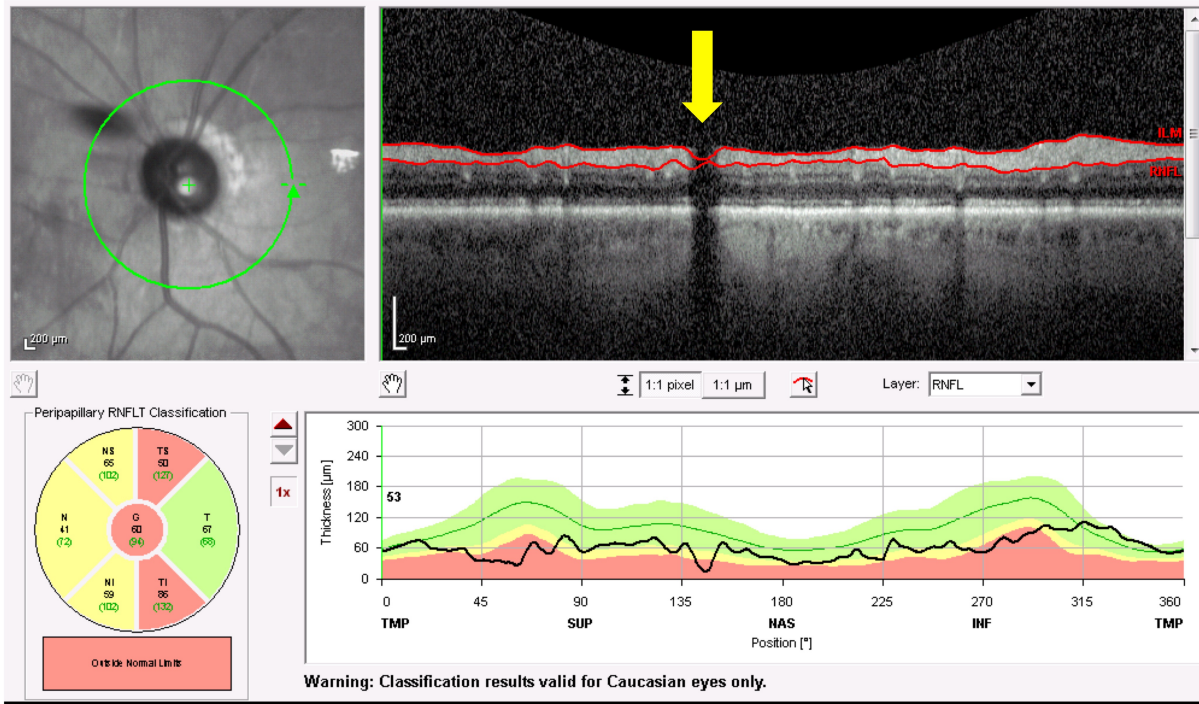


Figure 7. Example of a type 7 artifact in Spectralis optical coherence tomography imaging of retinal nerve fiber layer in glaucoma. A type 7 artifact is an image with abrupt lateral edge truncation of the retinal nerve fiber layer (yellow arrows).

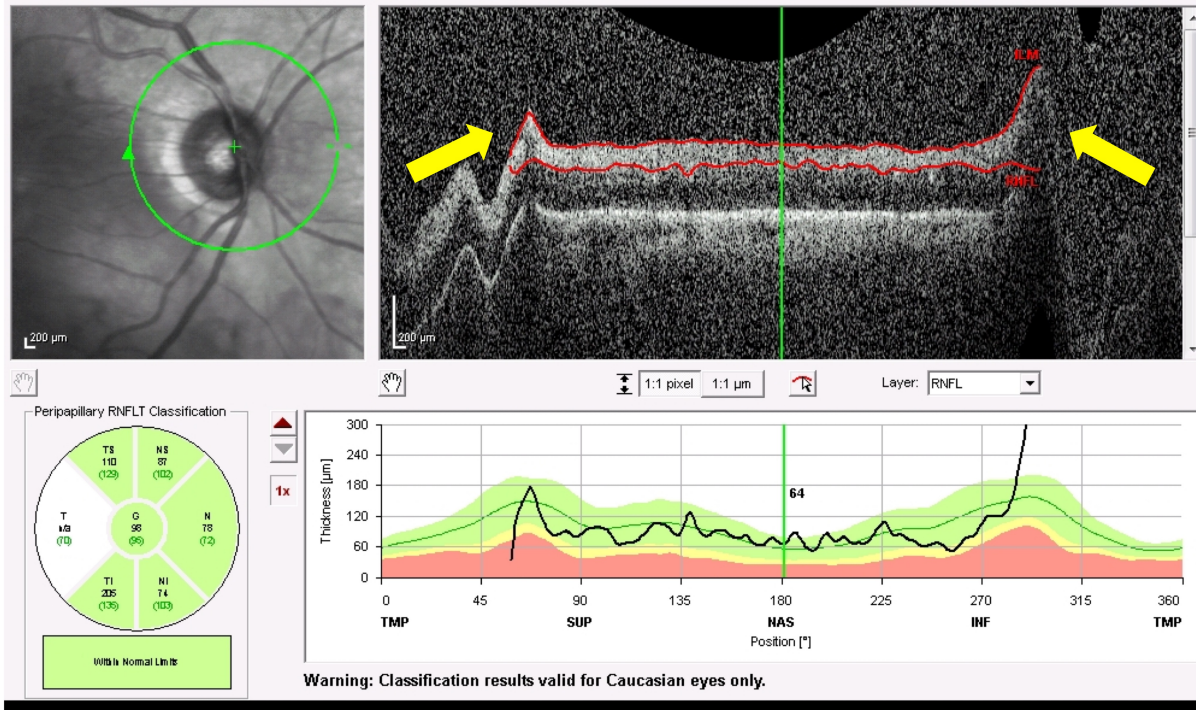


Figure 8. Example of a type 8 artifact in optical coherence tomography imaging of retinal nerve fiber layer in glaucoma. A type 8 artifact is when the retinal nerve fiber layer borders are blurred and out of the rectangular display printout due to patient movement.

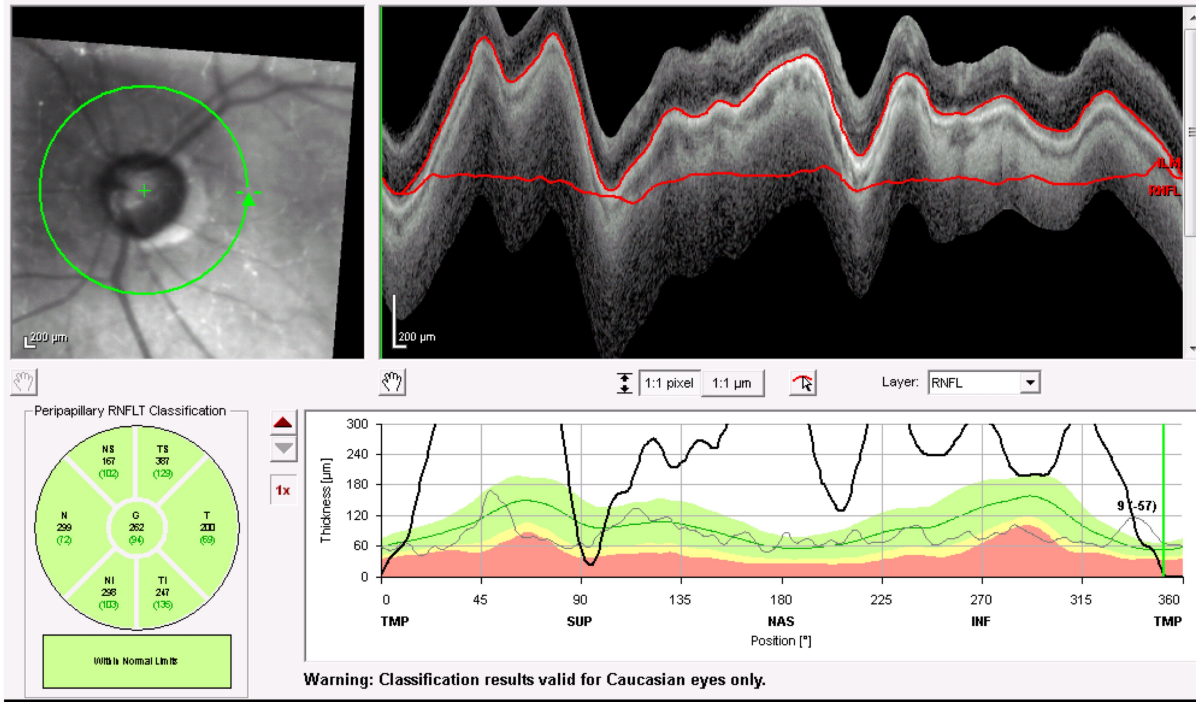


Figure 9. Example of a type 9 artifact in optical coherence tomography imaging of retinal nerve fiber layer in glaucoma. A type 9 artifact is due to a posterior vitreous detachment (yellow arrow).

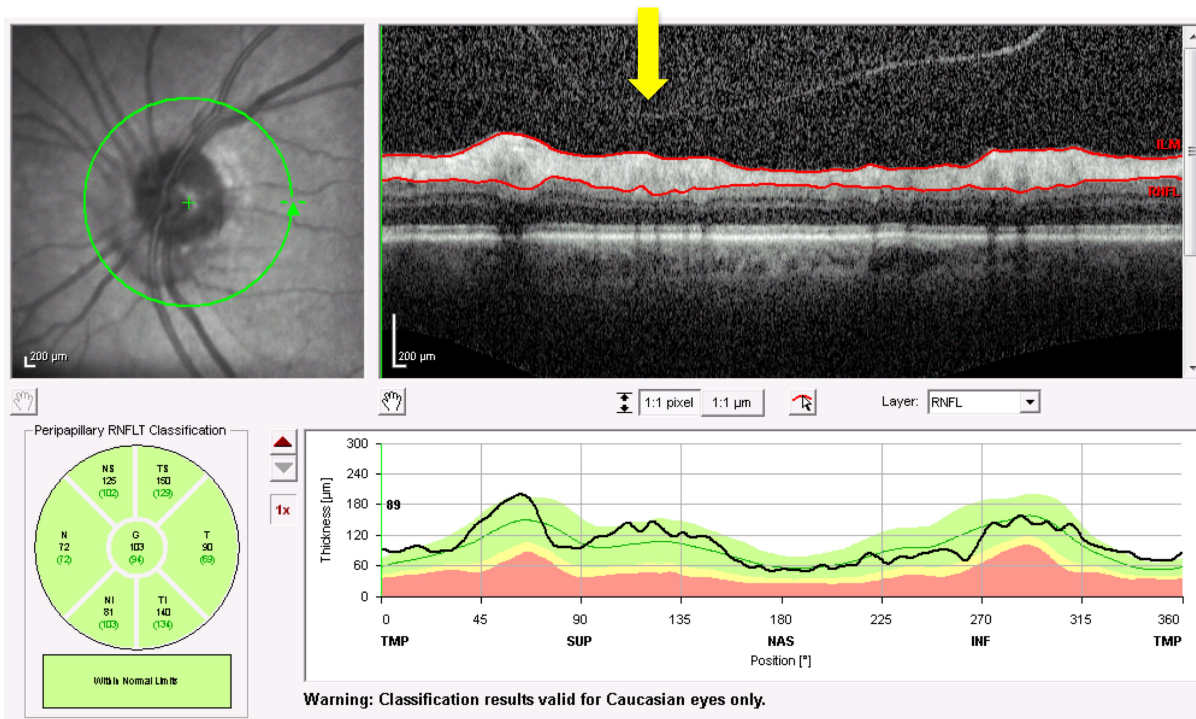


Figure 10. Example of a type 10 artifact in optical coherence tomography imaging of retinal nerve fiber layer in glaucoma. A type 10 artifact is due to peripapillary atrophy (yellow arrow).

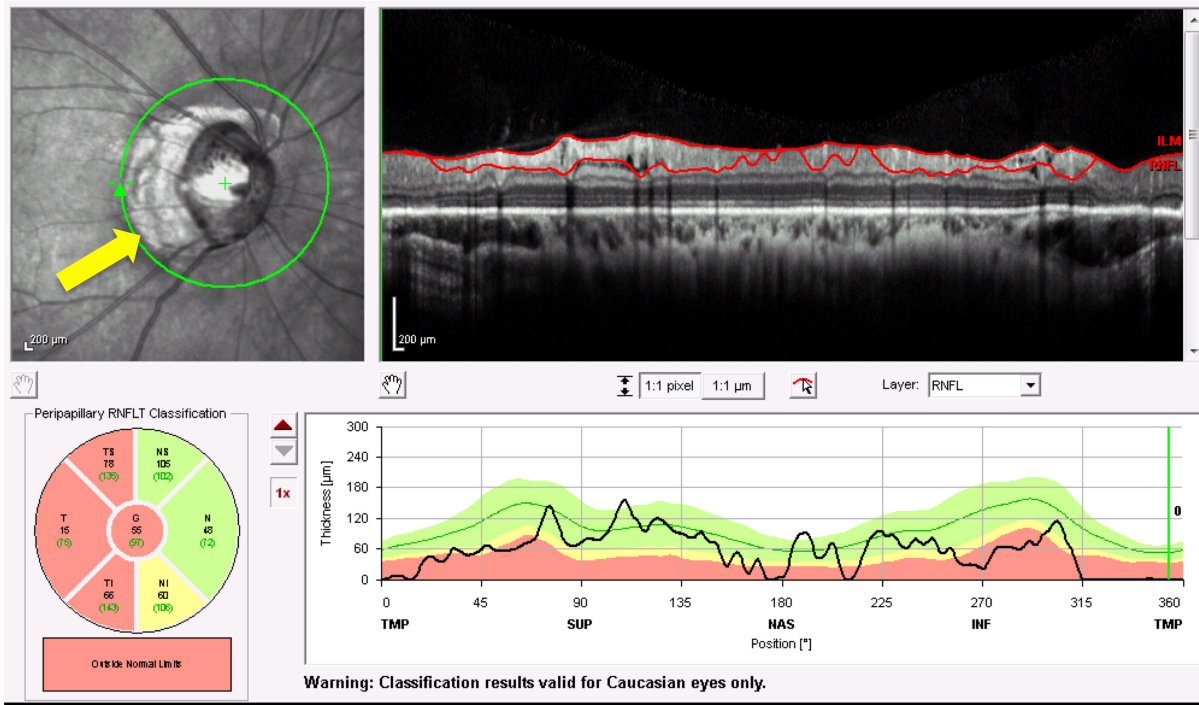


Figure 11. Example of a type 11 artifact in optical coherence tomography imaging of retinal nerve fiber layer in glaucoma. A type 11 artifact is due to a staphyloma (yellow arrow).

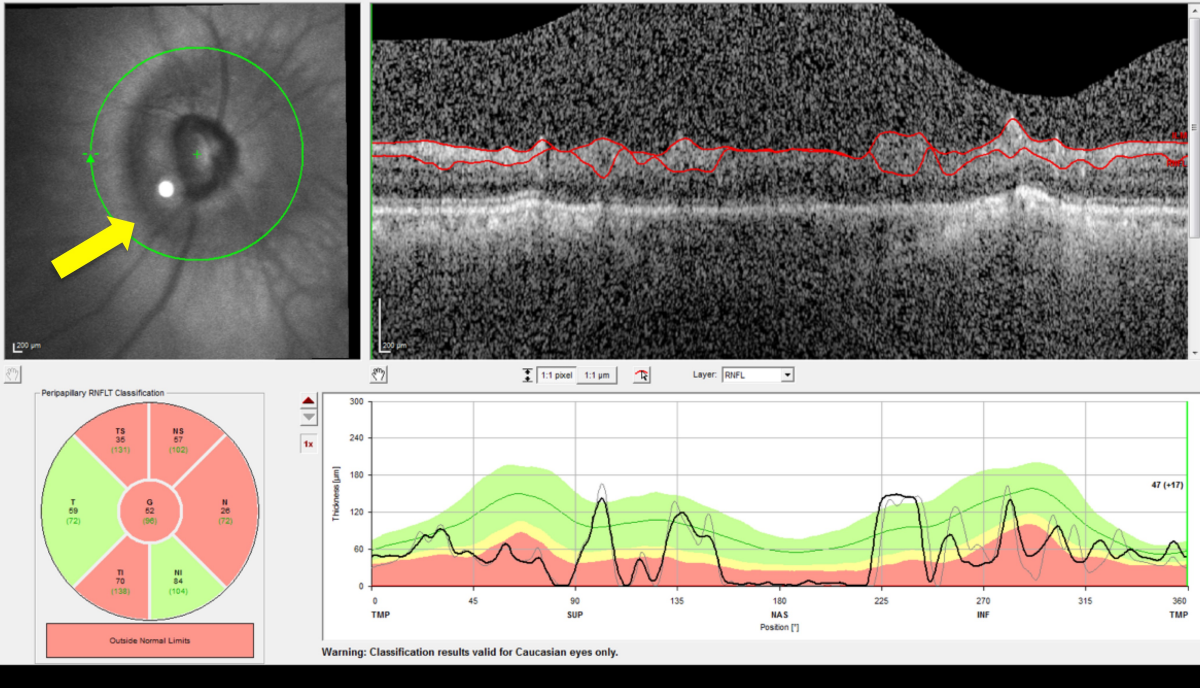


Figure 12. Example of a type 12 artifact in optical coherence tomography imaging of retinal nerve fiber layer in glaucoma. A type 12 artifact is due to myelinated nerve fibers (yellow arrow).

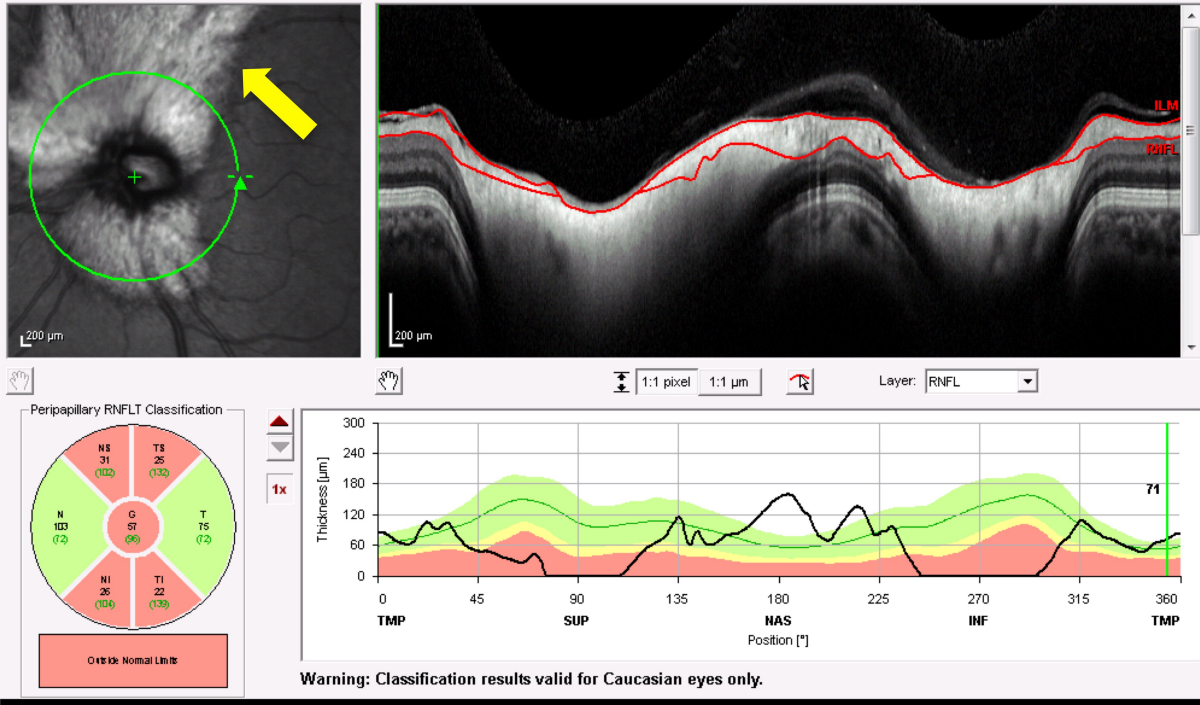
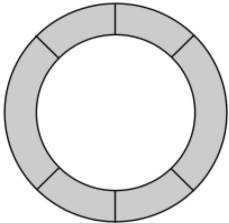
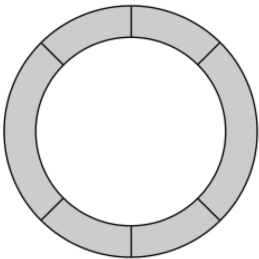


Figure 13. A schematic representation and definition of circumpapillary annulus (CA) 1 to 4.

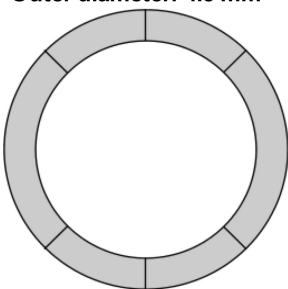
A CA1
Inner diameter: 2.5 mm
Outer diameter: 3.5 mm



B CA2
Inner diameter: 3.0 mm
Outer diameter: 4.0 mm



C CA3
Inner diameter: 3.5 mm
Outer diameter: 4.5 mm



D CA4
Inner diameter: 4.0 mm
Outer diameter: 5.0 mm

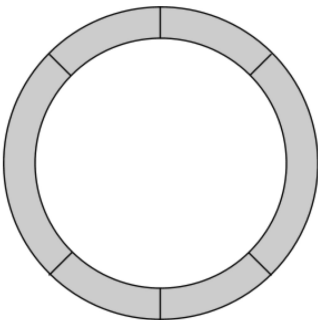


Figure 14. Annuli superposed on fundus. In-house MATLAB program conducts peripapillary retinal volume measurements in Spectralis volume scans by first centering circumpapillary annuli of pre-specified sizes on optic nerve head.

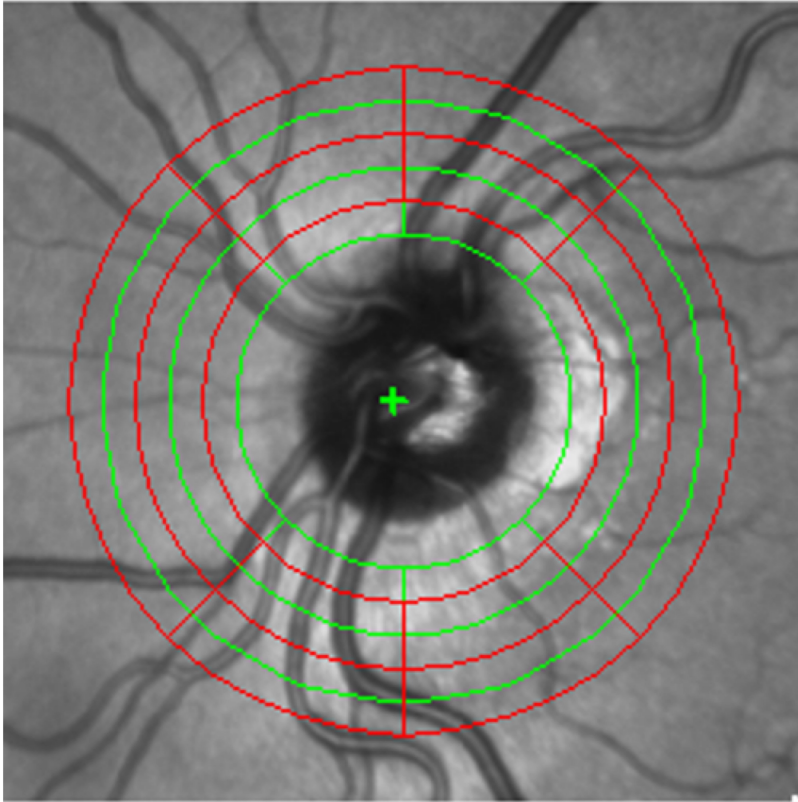


Figure 15. A schematic representation of quadrants and sectors/octants in a left eye: superior-temporal [ST], superior-nasal [SN], inferior-temporal [IT], inferior-nasal [IN].

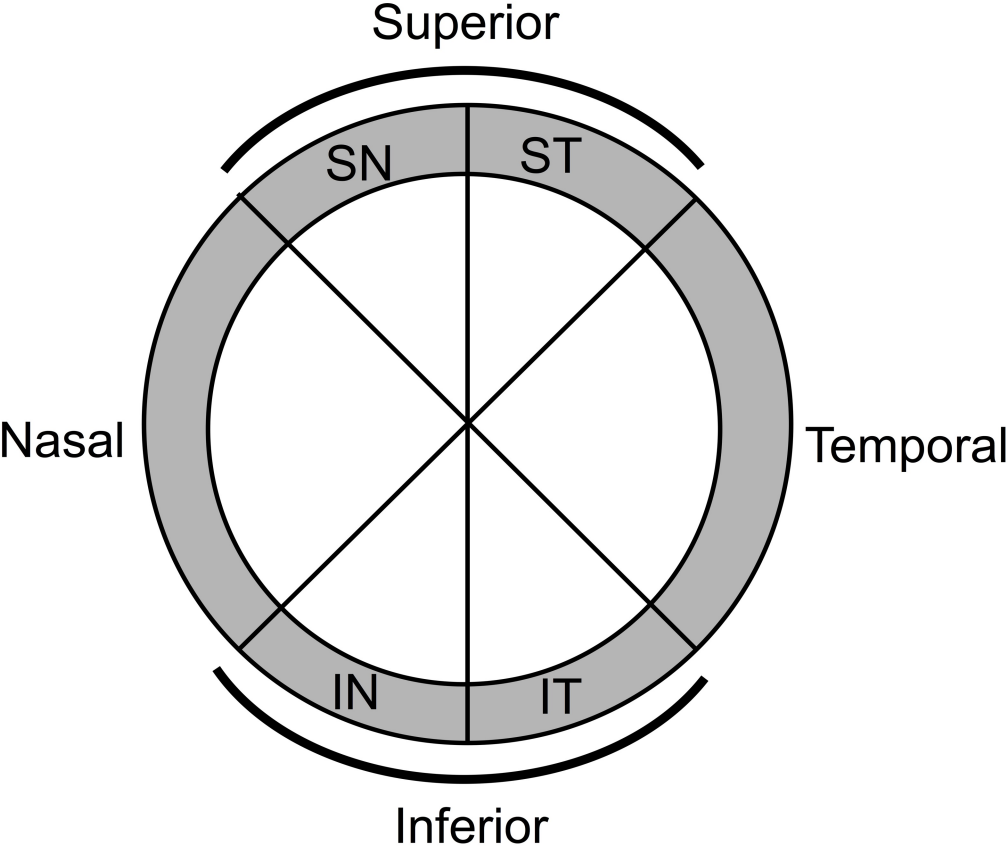


Figure 16. Automatic segmentation of the retina by an in-house MATLAB program which also conducts peripapillary retinal volume measurements in Spectralis volume scans. The red line delineates the internal limiting membrane, or the anterior border of the retina. The blue line delineates the retinal pigment epithelium/Bruch's membrane complex, or the posterior border of the retina.

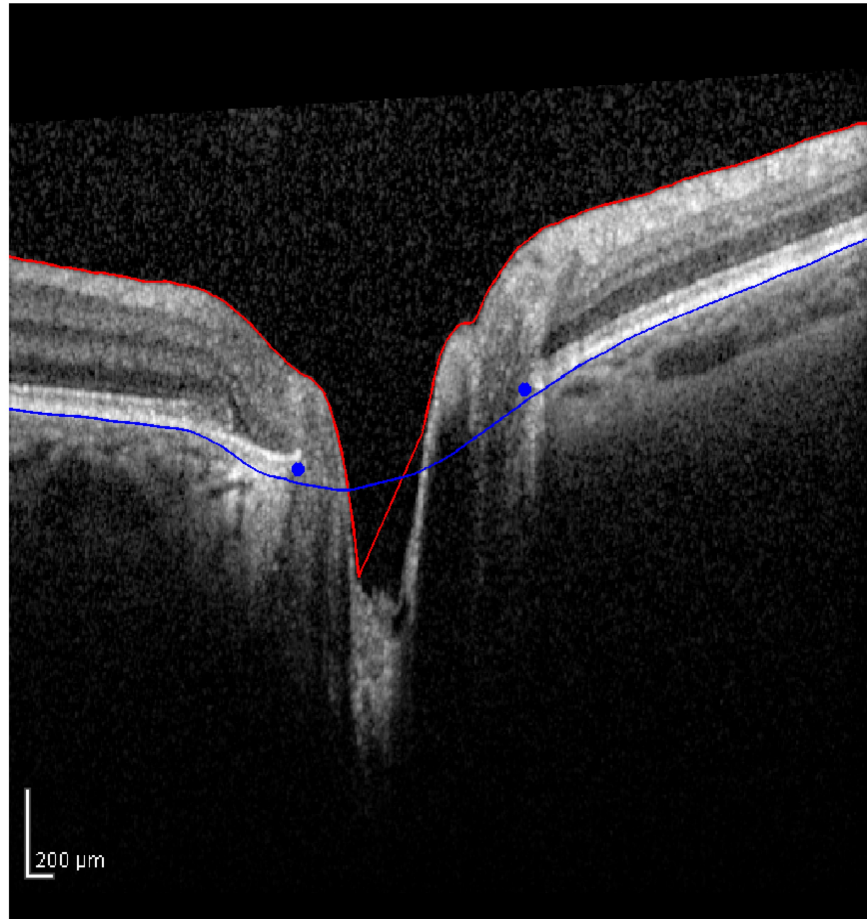


Figure 17. 3D retinal nerve fiber layer and retinal topography as generated by an in-house MATLAB program that conducts peripapillary retinal volume measurements in Spectralis volume scans.

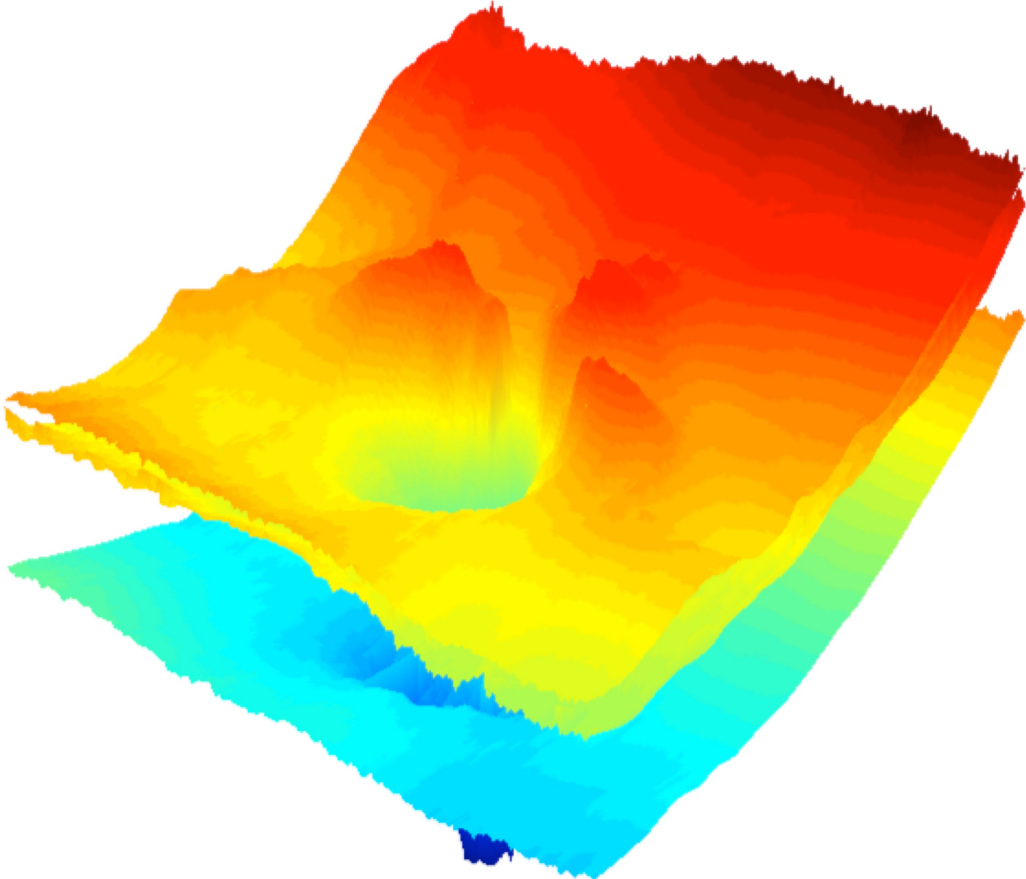


Figure 18. Example of anterior segmentation error in retinal volume scan by Spectralis OCT. Red line incorrectly segments anterior border of the retina, or internal limiting membrane, at the left end of the scan (yellow arrow).

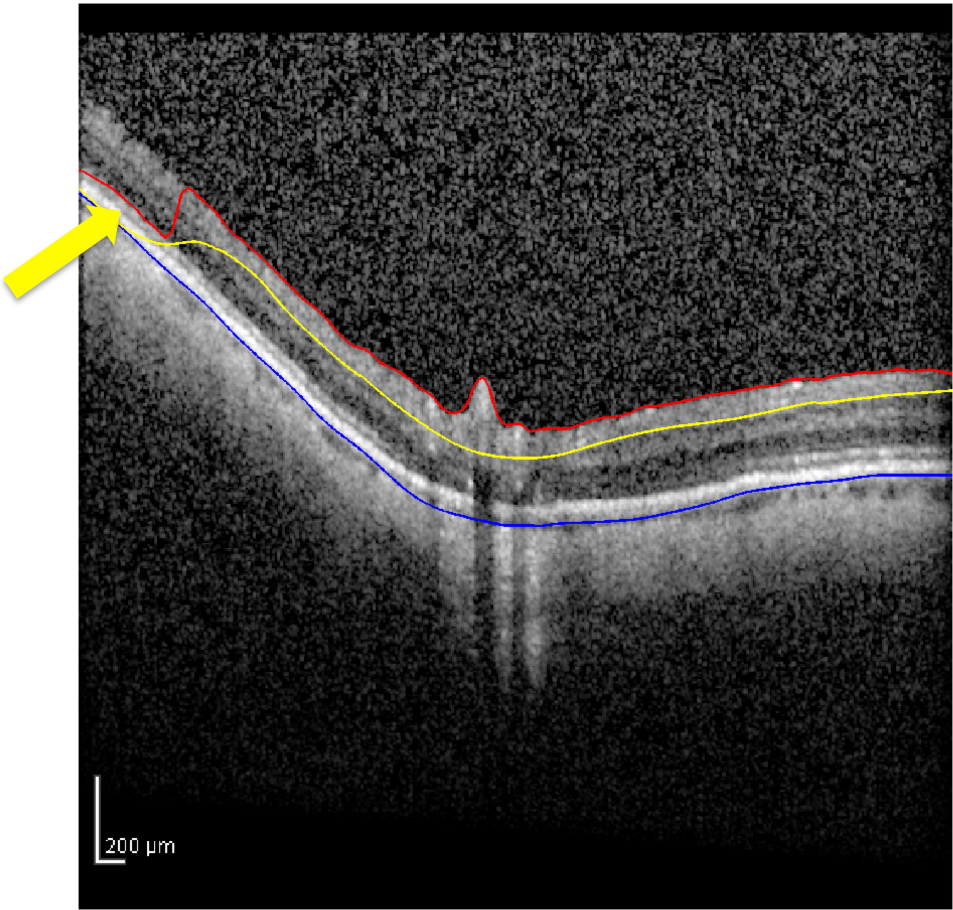


Figure 19. Example of posterior segmentation error in retinal volume scan by Spectralis OCT. Blue line incorrectly segments posterior border of the retina or retinal pigment epithelium/Bruch's membrane complex (yellow arrows).

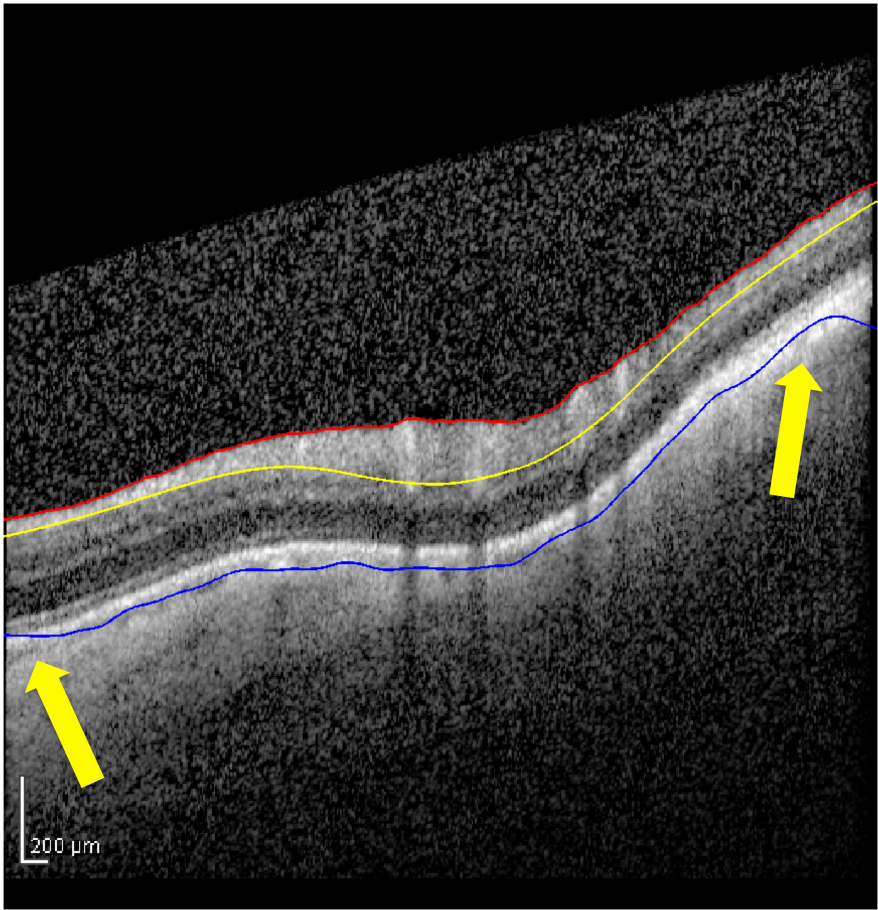


Figure 20. Example of missing part artifact in retinal volume scan by Spectralis OCT. It occurs when part of the scan is missing or when a portion of the RNFL across its entire thickness is completely black or has a poor signal-to-noise ratio.

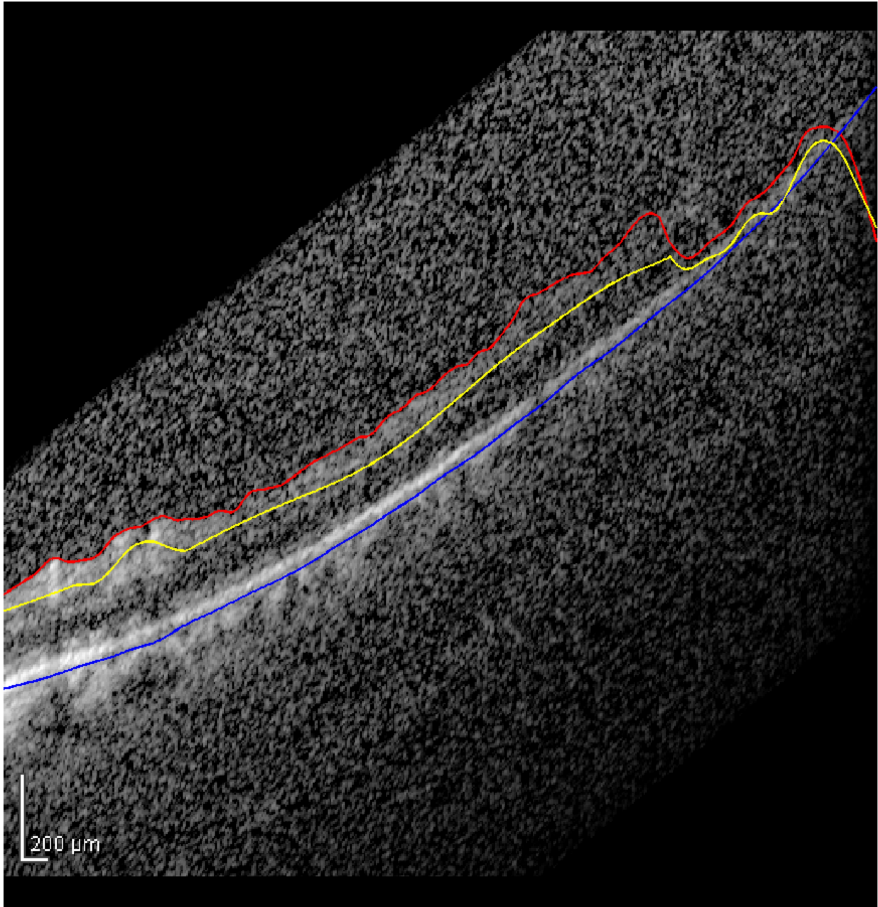


Figure 21. Example of cut edge artifact in retinal volume scan by Spectralis OCT. Cut edge artifacts are identified in cases of abrupt lateral edge truncation of the retina.

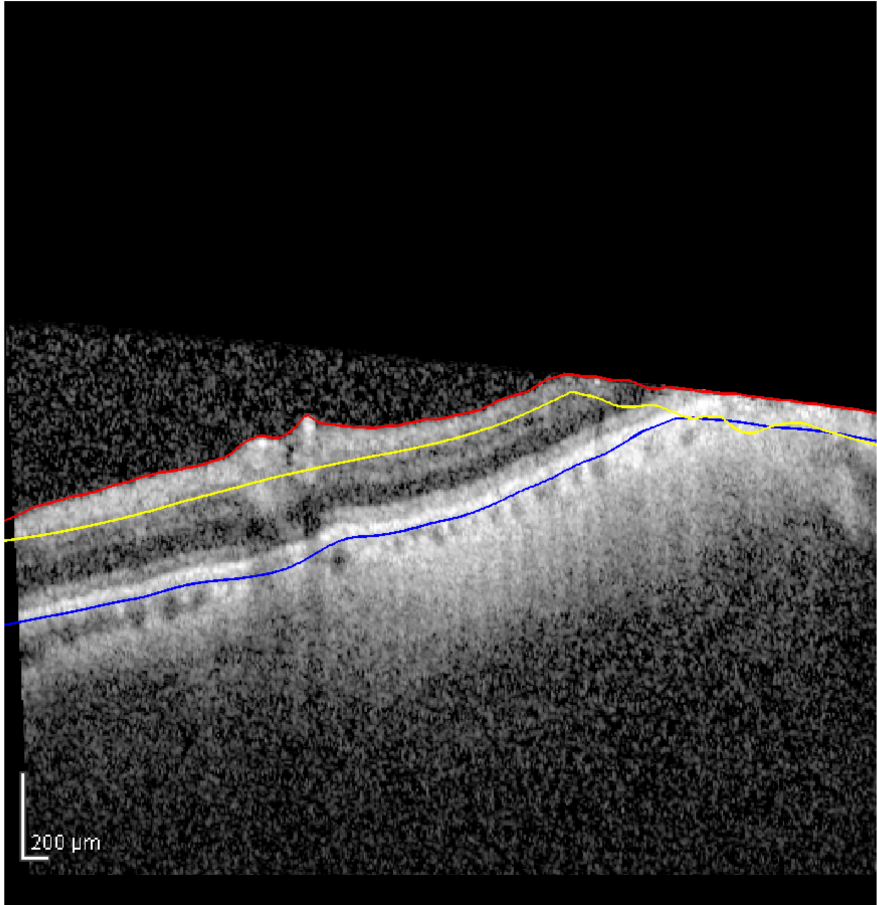


Figure 22. Example of mirror artifact in retinal volume scan by Spectralis OCT. Mirror artifact occurs when the retina is inverted and/or a ghost image is created from an out-of-register image.

